Published in final edited form as:
Geochim Cosmochim Acta. 2018 May 1; 228: 220–242. doi:10.1016/j.gca.2018.02.040.

Oxygen isotope systematics of chondrules in the Murchison CM2 chondrite and implications for the CO-CM relationship

Noël Chaumard[a,*], **Céline Defouilloy**[a], and **Noriko T. Kita**[a]

[a]WiscSIMS, Department of Geoscience, University of Wisconsin-Madison, 1215 W. Dayton Street, Madison, WI 53706-1692, USA

Abstract

High-precision oxygen three-isotope measurements of olivine and pyroxene were performed on 29 chondrules in the Murchison CM2 chondrite by secondary ion mass spectrometry (SIMS). The oxygen isotope ratios of analyzed chondrules all plot very close to the primitive chondrule minerals (PCM) line. In each of 24 chondrules, the olivine and/or pyroxene grains analyzed show indistinguishable oxygen isotope ratios. Exceptions are minor occurrences of isotopically distinguished relict olivine grains, which were found in nine chondrules. The isotope homogeneity of these phenocrysts is consistent with a co-magmatic crystallization of olivine and pyroxene from the final chondrule melts and a significant oxygen isotope exchange between the ambient gas and the melts. Homogeneous type I chondrules with Mg#'s of 98.9–99.5 have host chondrule $\Delta^{17}O$ values ranging from −6.0‰ to −4.1‰, with one exception ($\Delta^{17}O$: −1.2‰; Mg#: 99.6). Homogeneous chondrules with Mg#'s <96, including four type II chondrules (Mg# ~65–70), have $\Delta^{17}O$ values of around −2.5%. Five type I chondrules (Mg# ≥99) have internally heterogeneous oxygen isotope ratios with $\Delta^{17}O$ values ranging from −6.5% to −4.0%, similar to those of host chondrule values. These heterogeneous chondrules have granular or porphyritic textures, convoluted outlines, and contain numerous metal grains dispersed within fine-grained silicates. This is consistent with a low degree of melting of the chondrule precursors, possibly because of a low temperature of the melting event and/or a shorter duration of melting. The $\Delta^{17}O$ values of relict olivine grains in nine chondrules range from −17.9% to −3.4%, while most of them overlap the range of the host chondrule values.

Similar to those reported from multiple carbonaceous chondrites (Acfer 094, Y-82094, CO, CR, and CV), the $\Delta^{17}O$ ~−5% and high Mg# (≥99) chondrules, which might derive from a reduced reservoir with limited dust enrichments (~50× Solar System), dominate the population of chondrules in Murchison. Other chondrules in Murchison formed in more oxidizing environment (Mg#<96) with higher $\Delta^{17}O$ values of −2.5%, in agreement with the low Mg# chondrules in Acfer 094 and CO chondrites and some chondrules in CV and CR chondrites. They might form in environments containing the same anhydrous precursors as for the $\Delta^{17}O$ ~−5% and Mg# ~99 chondrules, but enriched in ^{16}O-poor H2O ice (~0.3–0.4× the CI dust; $\Delta^{17}0>0\%$) and at dust enrichments of ~300–2000×.

Regarding the Mg# and oxygen isotope ratios, the chondrule populations sampled by CM and CO chondrites are similar and indistinguishable. The similarity of these ^{16}O-rich components in CO

*Corresponding author. chaumard@wisc.edu.

and CM chondrites is also supported by the common Fe/Mn ratio of olivine in type II chondrules. Although they accreted similar high-temperature silicates, CO chondrites are anhydrous compared to CM chondrites, suggesting they derived from different parent bodies formed inside and outside the snow line, respectively. If chondrules in CO and CM chondrites formed at the same disk locations but the CM parent body accreted later than the CO parent body, the snow line might have crossed the the common chondrule-forming region towards the Sun between the time of the CO and CM parent bodies accretion.

Keywords

Carbonaceous chondrites; chondrules; oxygen three-isotope measurements; SIMS analyses

1. INTRODUCTION

CM (Mighei-like) chondrites are the most abundant group of carbonaceous chondrites (CCs) (Weisberg et al., 2006). They are primitive meteorite mostly of petrologic type 2 (e.g., McSween 1979; Kallemeyn and Wasson, 1981; Zolensky et al., 1993; Rubin et al., 2007), which derived from parent bodies that suffered significant aqueous alteration and low to mild thermal metamorphism (e.g., Sears and Dodd, 1988; Brearley and Jones, 1998; Brearley, 2003; and references therein; Busemann et al., 2007; Schrader and Davidson, 2017). CM chondrites, which can be considered as impact breccias, have been recognized as clasts in many other meteorite classes suggesting that CM chondrites may derive from multiple parent bodies, abundant and/or widely dispersed in the main belt (e.g., Zolensky et al., 1996; Gounelle et al., 2003; Bischoff et al., 2006; and references therein). Hence, CM chondrites are one of the most appropriate material to unravel the formation and evolution of the early Solar System.

CM chondrites display similarities to CO chondrites, though they are generally anhydrous, with respect to chemical compositions of anhydrous minerals (Frank et al., 2014; Schrader and Davidson, 2017) and refractory lithophile element abundances of the bulk chondrites (Kallemeyn and Wasson, 1981). Thus, they are sometime referred as CO-CM clan and considered to be closely related groups of chondrites (Kallemeyn and Wasson, 1981; Weisberg et al., 2006). The genetic relationship between CO-CM was also suggested on the basis of oxygen three-isotope systematics. According to oxygen three-isotope studies of CM chondrites by Clayton and Mayeda (1984, 1999), anhydrous minerals in the Murchison CM chondrite (i.e., chondrules) are more ^{16}O-rich than those in the bulk CM and similar to bulk CO chondrites, while Murchison matrix separates (i.e. phyllosilicates formed in low temperature fluid) are depleted in ^{16}O. Bulk CM chondrite data are on a mixing line between these two components with a slope of ~0.7 (Fig. 1). These results suggest that materials in CO chondrites would represent components in CM chondrites prior to parent body aqueous alterations.

Recent oxygen three-isotope data of CM falls (Greenwood et al., 2014) and the two lithologies (altered and less altered) of the Paris CM2 chondrite (Hewins et al., 2014) show a better-defined linear trend in $\delta^{18}O$-$\delta^{17}O$ plot that reinforces the mixing line suggested by

Clayton and Mayeda (1999). Hewins et al. (2014) obtained a line with a slope of 0.69 (R^2 = 0.93) and an intercept of −4.23‰ from a regression of CM falls, Paris, and CO falls that best represent bulk CM chondrite trend. Similar regression lines were reported from bulk and carbonate in CM chondrites (Benedix et al., 2003; Lindgren et al., 2017; Verdier-Paoletti, 2017), as well as from calcite analyses of Sutter's Mill (Jenniskens et al., 2012; slope of 0.62 and intercept of −4.88‰). As suggested by Jenniskens et al. (2012), the slopes of these regression lines higher than 0.52 strongly suggest mass independent fractionation by a water-rock reaction involving flowing water along a temperature gradient. The end points of these regression lines and the one from Hewins et al. (2014) pass through the field defined by the recent high precision oxygen three-isotope measurements of olivine and pyroxene from chondrules in the Yamato 81020 (Y-81020) CO3.0 chondrite performed by secondary ion mass spectrometers (SIMS; Tenner et al., 2013). These data may indicate that the anhydrous materials (i.e., high temperature silicates in chondrules; ^{16}O-rich) of CM chondrites are identical to those in CO3 chondrites. Further it has been debated whether CM and CO derived from a single parent body or from distinct parent bodies from common precursors (Greenwood et al. 2014).

To address these questions, we report *in situ* high precision SIMS oxygen three-isotope analyses on olivine and pyroxene in chondrules from the Murchison CM2 chondrite. In previous SIMS oxygen isotope studies of pristine chondrules, multiple olivine and/or pyroene analyses in a single chondrule are, in most cases, indistinguishable at the precision of SIMS analyses (0.3–0.5‰ in 2SD) except for "relict olivine" (e.g, Ushikubo et al., 2012; Tenner et al., 2013). In Acfer 094 (ungroup carbonaceous chondrite 3.00 with minimal aqueous alteration and metamorphism; Grossman and Brearley, 2005; Kimura et al., 2008), oxygen isotope ratios of glass and minerals in mesostasis are also indistinguishable from olivine and pyroxene phenocrysts in the same chondrules (Ushikubo et al., 2012). Thus, homogeneous oxygen isotope ratios in olivine and pyroxene in chondrules represent those of the chondrule melt during their formation, which has been referred as "host" chondrule oxygen isotope rarios. Using olivine and pyroxene to determine the "host" chondrule oxygen isotope ratios is particularly helpful for chondrules in mildly metamorphosed or aqueously altered chondrites, because olivine and pyroxene have slower oxygen isotope diffusion and are more resistant to hydration compared to glass and plagioclase in chondrule mesostasis. It is true for Murchison, in which chondrule mesostasis are altered to phylosilicates.

We further determine Mg# (= MgO/[MgO+FeO] in mol.%) of olivine and low-Ca pyroxene in individual chondrules that represent oxygen fugacity variations during chondrule formation (Ebel and Grossman, 2000; Tenner et al., 2015). Several studies have shown that oxygen isotope ratios of individual chondrules in each group of CCs vary against Mg# (Nakashima et al., 2010; 2011; Ushikubo et al. 2012; Schrader et al., 2013, 2014; 2017a; Tenner et al., 2013; 2015; 2017; Hertwig et al., 2017; 2018). Tenner et al. (2015) observed the monotonic increase of the Δ^{17}O (= $\delta^{17}0–0.52\times\delta^{18}0$) values of chondrules in CR chondrites with decreasing Mg#'s, which is interpreted as the result of a mixing between a ^{16}O-rich anhydrous dust (Δ^{17}O = −6‰) and ^{16}O-poor water ice (Δ^{17}O = +5‰) in the chondrule precursors. For Acfer 094 and CO chondrites, Δ^{17}O values of chondrules display a bimodal distribution of Δ^{17}O, with values of ~−5‰ and ~−2.5‰ for Mg#>98 and Mg#~99–30 chondrules, respectively (Ushikubo et al., 2012; Tenner et al., 2013). CV

chondrites and the Yamato 82094 (Y-82094) ungrouped CC are dominated by chondrules with lower $\Delta^{17}O$ values of ~−5‰ and high Mg# (>98), though some chondrules show higher $\Delta^{17}O$ and lower Mg#, similar to ~−2.5‰ chondrules in Acfer 094 and CO3 (Hertwig et al., 2017; 2018; Tenner et al. 2017). CH and CB chondrites are dominated by type I (FeO-poor: Mg#>90) chondrules with $\Delta^{17}O$ values of ~−2.5‰, which is very similar to those reported for CB chondrites (Krot et al. 2010; Nakashima et al., 2010; 2011), though CH chondrites contain chondrules with higher $\Delta^{17}O$ values of ~+1.5‰ and a wide range of Mg# (98–60) and lower $\Delta^{17}O$ values of ~−6‰ with high Mg# (≥98). In contrast, most chondrules in H, LL, R, and EH chondrites have $\Delta^{17}O$ values of 0–1% regardless of the Mg# (Kita et al., 2008, 2010, 2015; Weisberg et al. 2010, 2011), while a few chondrules show negative $\Delta^{17}O$ values but rarely below −4%. It thus appears that the chondrules with high Mg# (>~98) and $\Delta^{17}O$ values of around −5% were sampled by all groups of CCs, but not by the ordinary, enstatite, and R chondrites (e.g., Tenner et al. 2017).

CM chondrites are the last major group of CCs that are not fully investigated yet for detail Mg#−$\Delta^{17}O$ relationship among chondrules (e.g., Jabeen and Hiyagon, 2003; Chaumard et al., 2016; 2017; Schrader et al., 2017b). We examined a large suite of type I and type II chondrules from Murchison, which is one of the least altered CM chondrite (e.g., Busemann et al., 2007; Schrader and Davidson, 2017) in order to fully characterize oxygen isotope systematics. These data are used to discuss the environment of formation and the relationships between CO and CM chondrites. Such data are also important reference regarding the ongoing near-Earth asteroids sample return missions. Indeed, CM parent bodies accreted significant amount of water/ice and are widely disperse and abundant in the main belt (e.g., Bischoff et al., 2006), so potentially sampled by the Hayabusa2 and OSIRIS-REx missions.

2. ANALYTICAL PROCEDURES

2.1. Sample and chondrule selection

We selected and analyzed chondrules from three thin sections of the Murchison CM2 chondrite allocated by the Smithsonian Institution (USNM 5294–2, USNM 5587–2, and USNM 5587–5). Based on size, texture, and mineralogy, we tried to obtain a chondrule selection as representative as possible, while taking into account the minimum size required for SIMS analyses. Our selection includes 25 type I (Mg#≥90) chondrules (from ~200 μm to 1.2 mm in diameter), three type II (Mg#<90) chondrules (~400–500 μm in diameter), and one large fragment of a type II chondrule (~400 μm in size). Twelve type I chondrules are porphyritic olivine-pyroxene (POP; 20–80% modal olivine), seven are porphyritic olivine (PO; >80% modal olivine), and three are porphyritic pyroxene (PP; <80% modal olivine). Two type I chondrules are granular olivine (GO) and one is granular olivine-pyroxene (GOP). The type II chondrules are all PO in texture.

As in all groups of CCs, chondrules in CM chondrites are predominantly type I (e.g., Jones, 2012). In CM chondrites, it has been reported that ~95% of chondrules are porphyritics, and that 10–40% of these porphyritic chondrules are type II (Jones, 2012; and references therein). Our selection displays ~93% of porphyritic chondrules, ~16% of them being type II and is thus representative of those of CM chondrites. In addition, PO, POP, and PP

chondrules in our selection represent approximately 38%, 41%, and 10%, respectively, of the entire population of chondrules analyzed. These values are larger for PO chondrules and slightly lower for POP chondrules compared to CO chondrites (8% for PO and 69% for POP chondrules; Jones, 2012; and references therein).

2.2. Scanning electron microscopy and electron microprobe analysis

Backscattered electron (BSE), secondary electron (SE) imaging and energy dispersive X-ray spectrometry (EDS) analyses were performed using a Hitachi S-3400N scanning electron microscope (SEM) at the University of Wisconsin-Madison using an accelerating voltage of 15 kV. We identified in BSE and SE chondrules containing silicate grains with no cracks, pits, or inclusions of other minerals to be suitable for SIMS analysis.

Quantitative chemical analyses were obtained using a Cameca SXFive FE electron microprobe at the University of Wisconsin-Madison. Olivine and pyroxene analyses were performed with an accelerating voltage of 15 keV and a beam current of 20 nA. Counting times for the peak and background were 10 and 5 sec., respectively. Standards used were natural olivine and synthetic forsterite and enstatite (Mg, Si), jadeite (Na, Al), chromian augite (Ca), microcline (K), TiO_2 (Ti), synthetic Cr_2O_3 (Cr), fayalite (Fe), and synthetic Mn_2SiO_4 (Mn). We used a LTAP crystal for the analyses of Mg, Al, Si, and Na, a LPET crystal for Ca and K, a PET crystal for Cr and Ti, and a LLIF crystal for Mn and Fe. The Probe for EPMA™ (PFE) software was used for data reduction and matrix corrections (ZAF and $\phi_\rho(z)$). Based on EPMA measurements, we calculated the Mg# of each analysis. Errors on Mg#'s and chemical compositions reported throughout this manuscript correspond to two standard deviations (2SD).

2.3. SIMS oxygen three-isotope analysis

In situ oxygen three-isotope analyses of olivine and pyroxene in type I and II chondrules were performed in two sessions with the Cameca IMS 1280 at the WiscSIMS laboratory, University of Wisconsin-Madison. Analytical methods and conditions are similar to those reported by Kita et al. (2009, 2010). The primary Cs+ beam was tuned to produce a 15 μm (session #1) and 10 μm (session #2) diameter spot with a primary ion intensity of ~3 nA and ~1 nA, respectively. Using a 15 μm diameter spot, secondary ions of ^{16}O, ^{17}O, and ^{18}O were detected simultaneously with three Faraday cups (FC), with intensities of ~3.5×10^9, ~1.3×10^6, and ~7.5×10^6 counts per second (cps), respectively. FC amplifier resistors were 10^{11} Ω for ^{17}O and ^{18}O, and 10^{10} Ω for ^{16}O as in the previous studies (e.g., Kita et al. 2010). For the analysis session using a 10 μm diameter spot, secondary ion intensities of ^{16}O, ^{17}O, and ^{18}O decreased to ~1.5×10^9, ~5.5×10^5, and ~2.9×10^6 cps, respectively. In order to reduce the noise level of the FC amplifier for ^{17}O analyses below a 10^6 cps intensity, we replaced the resistor and capacitor pair on the FC amplifier board by a 10^{12} Ω resistor and 1 pF capacitor pair that were on the FC amplifier board from a Finnigan MAT 251 stable mass spectrometer. Typical thermal noise of FC amplifier (measured as 1SD of 4s integration) was reduced from 2,000 cps by using 10^{11} Ω resistor down to 1,200 cps by using 10^{12} Ω resistor. For the two sessions, the mass resolving power (MRP at 10% peak height) was set to ~2200 for ^{16}O and ^{18}O using two detectors on the multi-collection array, and 5000 for ^{17}O using a fixed mono-collector (axial detector). At the end of each analysis, ^{16}OH was measured to

determine its contribution to the ^{17}O signal following the methods described by Heck et al. (2010). The correction of the ^{17}O signal from ^{16}OH was negligible (<0.08‰) for both standards and unknowns, except for a few cases as high as 0.2% in unknowns.

Measured $^{18}O/^{16}O$ and $^{17}O/^{16}O$ ratios were normalized to the VSMOW scale ($\delta^{18}O$ and $\delta^{17}O$ that are expressed as a deviation from standard mean ocean water in the unit of 1/1000; Baertschi, 1976). The external reproducibility has been determined by intermittent measurements of a San Carlos (SC) olivine standard ($\delta^{18}O$ = 5.32%; Kita et al., 2010). We performed 8 SC olivine analyses, 4 before and 4 after, to bracket 9 to 19 unknown chondrule analyses (Kita et al., 2009). External reproducibility is calculated as the 2SD of the SC olivine brackets, with average values during session #1 (15 μm) of 0.2‰, 0.3‰, and 0.3‰ for $\delta^{18}O$, $\delta^{17}O$, and $\Delta^{17}O$, respectively. For session #2 (10 μm), the 2SD average values are 0.3‰, 0.5‰, and 0.5‰ for $\delta^{18}O$, $\delta^{17}O$, and $\Delta^{17}O$, respectively. As discussed by Kita et al. (2009), they represent the spot to spot reproducibility and were thus assigned as the uncertainties of each individual spot analysis.

Corrections for instrumental biases of unknown olivine and pyroxene analyses due to their chemical compositions (EA1) were estimated by measuring olivine ($Fo_{60–100}$), low-Ca pyroxene ($En_{70–97}$), and diopside (Wo_{50}) standards with known oxygen isotope ratios (e.g., Kita et al., 2010; Tenner et al., 2015). The calibration curves were normalized relative to the bias of the SC olivine bracketing standard (EA1) that were analyzed repeatedly throughout the analysis sessions. The compositional ranges of standards cover those of unknowns measured, with the exception of 2 type II chondrules that contain FeO-rich olivine grains with compositions of ~Fo_{50}. Although these olivine grains may have systematic errors in $\delta^{18}O$ and $\delta^{17}O$ due to extrapolated instrumental bias corrections, those errors are mass-dependent and would not affect the $\Delta^{17}O$ values.

In order to determine host chondrule oxygen isotope ratios, we obtained multiple SIMS analyses per chondrule (n= 6 to 11, average: 8). This number of measurement for each chondrule is necessary to confirm multiple analyses with indsitiguishable $\Delta^{17}O$ values determining the host chondrule values. Many CC chondrules contain olivine grains with heterogeneous oxygen isotope ratios (Kunihiro et al., 2004a, 2005; Wasson et al., 2004; Connolly and Huss, 2010; Rudraswami et al., 2011; Ushikubo et al., 2012; Schrader et al., 2013; 2017a; Tenner et al., 2013). These olivine grains with distinct isotope ratios are commonly considered as “relict” and are likely unmelted crystals that survived during the final high-temperature event of the chondrule formation. They preserved oxygen isotope ratios due to the slow diffusivity of oxygen isotopes (e.g., Chakraborty, 2010). These relict grains were not used to determine the averaged “host” oxygen isotope ratio of each chondrule that is thus considered as representative of the final chondrule melt from which “non-relict” olivine and pyroxene grains crystallized. As defined by Ushikubo et al. (2012) and Tenner et al. (2013, 2015), we define relict olivines those with $\Delta^{17}O$ values exceeding the average 3SD external reproducibility (0.50‰ and 0.75‰, for sessions 1 and 2, respectively) when compared to the average “host” $\Delta^{17}O$ value of the considered chondrule.

Uncertainties of averaged host $\delta^{18}O$ and $\delta^{17}O$ for each chondrule are taken as the propagation of (i) the 2 standard error (2SE) of chondrule analyses (=2SD/√number of

analyses), (ii) the 2SE of associated SC olivine bracketing analyses that are used for bias corrections, and (iii) the uncertainty due to the sample topography and/or sample positioning on the SIMS stage as well as uncertainty of instrumental bias corrections, estimated to be 0.3% for $\delta^{18}O$ and 0.15% for $\delta^{17}O$ (Kita et al., 2009). Since (iii) is mass-dependent and does not affect $\Delta^{17}O$, the propagated uncertainty in $\Delta^{17}O$ only uses (i) and (ii). For relict grains, the uncertainties are the spot-to-spot reproducibility (2SD) as determined by bracketing analyses of SC olivine.

After the two SIMS sessions, we checked each spot analysis using SEM-BSE-SE images. Three of 233 pits either overlapped cracks, imperfections, and/or different phases, or displayed a contribution of ^{16}OH to the ^{17}O signal of ≥0.1%, and were rejected from our final dataset.

3. RESULTS

BSE images of representative chondrule textures and chemistries are shown in Fig. 2a-2d. BSE images of all chondrules, in which we reported SIMS pits and analyses numbers, are shown in EA2. Electron microprobe analyses and oxygen isotope measurements are summarized in EA3 and EA4, respectively.

3.1. Texture, petrography, and mineralogy of chondrules

In porphyritic type I chondrules, olivine grains are present either as euhedral grains (from ~5 μm to ~100 μm), large anhedral phenocrysts, or both. Olivine is mostly located in the central parts of these chondrules, while low-Ca pyroxene is abundant at the periphery. The low-Ca pyroxene often displays a poikilitic texture and contains numerous pores and cracks, probably formed during the protoenstatite-clinoenstatite transition (Hanowski and Brearley, 2001). Low-Ca pyroxene was also observed as large euhedral grains (~40 μm width and up to ~150 μm length). High-Ca pyroxene grains typically surround low-Ca pyroxene grains, with sizes ranging from a few μm to ~70 μm length. In porphyritic type I chondrules, olivine grains are chemically homogeneous, with an average Mg# of 99.3±0.4 (98.6–99.7). They contain 0.29±0.17 wt% CaO, 0.38±0.25 wt% Cr_2O_3, and up to 0.48 wt% Al_2O_3. The Mg#'s calculated for low-Ca pyroxene grains range from 98.9 to 99.5, with an average composition of low-Ca pyroxene of $En_{97.5\pm2.4}Fs_{0.8\pm0.2}Wo_{1.7\pm2.3}$. We measured 0.39–1.87 wt% Al_2O_3 and 0.30–0.72 wt% Cr_2O_3. The average composition of high-Ca pyroxene is $En_{60.3\pm10.2}Fs_{0.8\pm0.4}Wo_{38.9\pm10.5}$, with Mg#'s ranging from 98.4 to 99.1. We measured significant amounts of TiO_2 (0.41–1.20 wt%), Cr_2O_3 (0.59–1.16 wt%), MnO (0.15–0.45 wt %), and Al_2O_3 (0.93–9.21 wt%).

We recognized three granular type I chondrules (chondrules B6, C8, and C10), which are composed of evenly sized grains with sparse mesostasis (Fig. 2b,c), especially near the borders. The Mg#'s of olivine and low-Ca pyroxene in granular type I chondrules range from 96.0 to 99.4 and from 95.4 to 99.3, respectively. Olivine grains contain 0.27±0.03 wt% CaO, 0.44±0.27 wt% Cr_2O_3, and up to 0.47 wt% MnO. The compositions of low-Ca pyroxene range between $En_{90.0}Fs_{4.4}$ and $En_{97.9}Fs_{0.7}$. We measured significant amount of Al_2O_3 (1.15–4.39 wt%), Cr_2O_3 (0.46–1.79 wt%), as well as 0.08–35 wt% TiO_2 and 0.14–

1.06 wt% MnO. Although chondrules B6 and C10 contain few grains of high-Ca pyroxene, they were two small to obtain quantitative analyses.

In type I chondrules, small inclusions of metal (<10 μm in size) were observed within euhedral olivine grains. In the center of some type I chondrules, large blebs (larger than ~30 μm in size) display a core of metal surrounded by a mixture between an abundant S-Fe-rich phase and, to a lesser extent, a Fe-rich phyllosilicate. This PCP (Poorly Characterized Phases) -like material (intergrowths of cronstedtite and tochilinite; e.g., Mackinnon and Zolensky, 1984; Tomeoka and Buseck, 1985; Browning et al., 1996) was commonly observed replacing metal in CM type I chondrules. In addition, and based on EDS analyses, the altered mesostasis of type I chondrules mainly consist of phyllosilicates (i.e., “spinach” phase; e.g., Fuchs et al., 1973).

The type II chondrules investigated have a porphyritic texture. Olivine phenocrysts display various degrees of aqueous alteration. They are almost fresh and unaltered in chondrule C12, and partially serpentinized (e.g., Lee and Lindgren, 2016) in chondrule B8. Mesostasis of type II chondrule is composed of phyllosilicates, as well as secondary ferroan olivine (rounded grains, <10 μm in size) in chondrule B9. The Mg# measured for olivine is variable from one grain to another in a single chondrule, as well as from one chondrule to another. The range of Mg# are 53.0–71.3, 63.2–71.7, 53.1–78.3, and 62.6–96.0 for chondrule C12, B9, C11, and B8, respectively. Olivine grains also contain significant amounts of Cr_2O_3 (0.22–0.52 wt%) and MnO (0.12–0.51 wt%).

3.2. Chondrule Mg#

In 19 of the 29 chondrules analyzed, we were able to compare Mg#’s of coexisting olivine and low-Ca pyroxene grains. As shown in Fig. 3, these 19 chondrules contain olivine and low-Ca pyroxene with similar Mg#’s. The 10 other chondrules contain either olivine or pyroxene grains. While the Mg# in olivine and pyroxene from chondrules show a wide range (~50–99), the consistency between olivine and low-Ca pyroxene Mg#’s within a single chondrule indicates they did not suffer significant secondary parent body processes such as thermal metamorphism and aqueous alteration (e.g., Jones, 1994; Tachibana et al., 2003; Ushikubo et al., 2012; Tenner et al., 2013, 2015; Schrader and Davidson, 2017; Schrader et al., 2017a). Because olivine and low-Ca pyroxene are the most abundant phases in chondrules investigated, we calculated the Mg# of individual chondrules defined as the average of its constituent olivine and/or low-Ca pyroxene excluding relict grains (Ushikubo et al., 2012; Tenner et al., 2013, 2015; 2017). Five chondrules investigated (the four type II chondrules and the type I GOP chondrule C8) have Mg#’s ranging between 64.9 and 96.0, while the other 24 chondrules have Mg#’s ranging from 98.9 to 99.6. The chondrule Mg#’s are given in Table 1.

3.3. Oxygen isotope ratios

We collected a total of 230 spots analyses from 29 chondrules from three sections in two separated sessions (15 and 10 μm beam size; EA4). Regardless of which mineral phase was measured, our data plot between the CCAM (carbonaceous chondrite anhydrous mineral; Clayton et al., 1977) and the Y&R (Young and Russell, 1998) lines, close to the PCM

(primitive chondrule minerals; Ushikubo et al., 2012) line, as shown in the examples of Fig. 2e-2h. The $\delta^{18}O$ and $\delta^{17}O$ values of olivine range from −34‰ to +5‰ and from −36‰ to +1‰, respectively, while those of pyroxene range from −7‰ to +3‰ and from −10‰ to +0‰, respectively (Fig. 4). Olivine data extend to lower $\delta^{18}O$ and $\delta^{17}O$ values compared to those of pyroxene because they include ^{16}O-rich relict olivine data as indicated below. Two analyses of olivine (spots #231 in chondrule B5 and #205 in chondrule A7; EA4) display unusual large internal errors for $\delta^{18}O$ and $\delta^{17}O$ (≥1 ‰). Cycle data plot along a slope 1 line supporting a variation of the oxygen isotope ratios (≥10‰ in $\delta^{18}O$ and $\delta^{17}O$) with depth, possibly due to the presence of small μm-sized ^{16}O-rich domains within the analysis spots.

In 19 chondrules, the $\Delta^{17}O$ values of multiple analyses within a chondrule agree within ±3SD external reproducibility (0.50‰ and 0.75‰ for 15μm and 10μm spot analyses, respectively), as shown in Fig. 2k-2l. Of these 19 chondrules, four chondrules (A4, A8, B3, C10) show a significant variability in $\delta^{18}O$ and $\delta^{17}O$ values (2–3%) beyond typical analytical uncertainty (e.g., Fig. 2g, 2k for C10). Their $\delta^{18}O$ and $\delta^{17}O$ values plot along the PCM line with the slope close to unity (0.84–0.91) and coefficients of determination (R^2) of 0.74–0.94 (EA4), indicating these three chondrules are internally heterogeneous in ^{16}O. Therefore, the host chondrules oxygen isotope ratios are calculated from the mean of multiple analyses in each chondrule except for A4, A8, B3, and C10.

In the other 10 chondrules, one or more olivine analyses show $\Delta^{17}O$ value(s) that differ more than 3SD external reproducibility. In most cases, by excluding between one and three olivine data, other coexisting olivine and/or pyroxene measurements are indistinguishable (Fig. 2i-2j). As described in 2.3, these isotopically distinct olivine grains are considered to be “relict” and excluded from the calculation of individual host chondrule values. In chondrule A6, five olivine grains display homogeneous isotope ratios ($\Delta^{17}O$ = −5.5‰), which differ significantly from those in two low-Ca pyroxene grains ($\Delta^{17}O$ = −4.1‰). As in the previous study (chondrule Y22 from Tenner et al. 2013), olivine in A6 are considered to be relict and the mean of pyroxene data is used to estimate the host chondrule data. In chondrule A7, $\Delta^{17}O$ values show a significant range from −6.2‰ to −4.6‰, even excluding two most ^{16}O-rich olivine data ($\Delta^{17}O$; −12.8‰ and −8.0‰). This chondrule is considered to be heterogeneous in oxygen isotopes and reliable host value cannot be determined.

In Table 1, oxygen isotope ratios of host chondrules are calculated from 24 chondrules (excluding the five heterogeneous chondrules A4, A7, A8, B3, C10). The texture, Mg#, the number of measurements per mineral, and the relict olivine analyses in the same chondrules are listed together. Individual spot analyses for the five heterogeneous chondrules are listed in Table 2. Host chondrule $\Delta^{17}O$ values along with their relict olivine analyses are summarized in Fig 5, which also shows individual data from five heterogeneous chondrules. Host chondrule $\Delta^{17}O$ values show discrete ranges; most type I chondrules (18 out of 20) range between −6.0‰ to −4.1‰, while five chondrules including all four type II chondrules show a small range of $\Delta^{17}O$ values between −2.6±0.2‰ and −2.3±0.2‰. The highest $\Delta^{17}O$ value of-1.2±0.2‰ is found from the type I POP chondrule C6. These ranges are very similar to those observed from Acfer 094 and CO3 (Ushikubo et al. 2012; Tenner et al. 2013). The $\Delta^{17}O$ values of relict olivine analyses (19 data from 9 chondrules) and individual analyses from five heterogeneous chondrules are mainly distributed between −6.5‰ and

−4.0‰, identical to host values from majority of type I chondrules. Several relict olivine analyses are between −6‰ and −8‰, which are within a range of host chondrules in type I chondrules from other CCs, such as Acfer 094, CV, CO, and Y-82094 (Libourel and Chaussidon, 2011; Ushikubo et al., 2012; Tenner et al., 2013, 2017; Hertwig et al. 2018). Only two analyses are significantly below $\Delta^{17}O<-8‰$; relict olivine in B6 (−17.9‰) and the most ^{16}O-rich analysis in A7 (−12.8‰). Similar ^{16}O-rich relict olivine data have been reported in chondrules in CCs (e.g., Ushikubo et al., 2012; Schrader et al., 2013; Tenner et al., 2013, 2017).

The host $\Delta^{17}O$ values of individual chondrules are correlated to their Mg#, as shown in Fig. 6. The lowest $\Delta^{17}O$ values correspond to the highest Mg#'s. The $\Delta^{17}O$ values range from −6.0‰ to −4.1‰ for Mg#'s ranging from 99.5 to 98.9, and from - 2.7±0.3‰ to −2.3±0.2‰ for Mg#'s ranging from 96 to 65. Only chondrule C6 deviates from this relationship with highest $\Delta^{17}O$ of −1.2% and highest Mg# of 99.6 (Fig. 6).

4. DISCUSSION

4.1. Oxygen isotope ratios of host chondrules

4.1.1. Co-origin of olivine and pyroxene—Excluding relict grains, most of the porphyritic type I chondrules analyzed are composed of olivine and low-Ca pyroxene with indistinguishable $\Delta^{17}O$ values. In the previous SIMS oxygen isotope studies of chondrules from various groups of CCs, multiple analyses of olivine and pyroxene phenocrysts within single chondrules show homogeneous oxygen isotope ratios within analytical uncertainties (e.g., Rudraswami et al., 2011; Ushikubo et al., 2012; Tenner et al., 2013, 2015, 2017; Zhang et al., 2014; Schrader et al., 2017a; Hertwig et al. 2018). Such observation suggests that coexisting pyroxene and olivine grains crystallized from isotopically homogeneous melts formed during the final melting event. Consistent oxygen isotope ratios between olivine and pyroxene are clearly demonstrated in Fig. 7 that plot $\delta^{18}O$, $\delta^{17}O$, and $\Delta^{17}O$ values of pyroxene against olivine on 1:1 lines, respectively. Similar 1:1 relationship between olivine and pyroxene from 15 individual chondrules has been reported from several groups of CCs (Rudraswami et al. 2011; Ushikubo et al. 2012; Tenner et al. 2012; 2015; 2017; Hertwig et al. 2018). According to these results, pyroxene and most of the olivine grains in these 15 chondrules from Murchison must have crystallized from the same final silicate melt that was homogeneous in oxygen isotopes.

Alternatively, several studies suggest that olivine from differentiated planetesimals would have been the precursors of type I chondrules in CV and CR chondrites and experienced gas-melt interactions during chondrule formation (Tissandier et al., 2002; Libourel et al., 2006; Chaussidon et al., 2008; Libourel and Chaussidon, 2011). Chaussidon et al. (2008) reported regression lines with slopes of ~0.8 for $\delta^{18}O$ and $\delta^{17}O$ values between olivine and pyroxene, respectively. Under this scenario, most of olivine in type I chondrules would be relicts and enriched in ^{16}O, while pyroxene formed as a result of high-temperature reactions between the silicate melt and ^{16}O-poor SiO molecules in the ambient gas (Marrocchi and Chaussidon, 2015). Co-existing olivine and pyroxene data in type I chondrules from Murchison do not show significant differences (≤0.8‰, ≤0.9‰, and ≤0.7‰ for $\delta^{18}O$, $\delta^{17}O$, and $\Delta^{17}O$, respectively; Fig. 7), thus do not support this scenario. Similarly, previous SIMS

studies of chondrules in other CCs including CV and CR chondrites (e.g., Rudraswami et al., 2011; Ushikubo et al., 2012; Schrader et al., 2017a; Tenner et al., 2013, 2015, 2017; Hertwig et al. 2018) all show consistent oxygen isotope ratios between olivine and pyroxene within a single chondrule. Thus, olivine is not systematically ^{16}O-rich compared to the coexisting pyroxene in most chondrules.

In CR chondrites, Schrader et al. (2013, 2014; 2017a) observed that the range of Δ^{17}O values measured for olivine phenocrysts in barred olivine (BO) chondrules are similar to those in porphyritic chondrules, while it is generally considered that BO chondrules were completely melted above the liquidus and porphyritic chondrules did not. Schrader et al. (2014) conclude that porphyritic chondrules do not retain abundant relict olivine grains, which is consistent with our observations. This is also an important argument against the origin of olivine as relict fragments of early-formed planetesimals.

4.1.2. Complete oxygen isotope exchange between ambient gas and chondrule melt—

As first indicated by Clayton (1983), it has been hypothesized that an incomplete isotope exchange between two distinct isotope reservoirs, ^{16}O-rich dust and ^{16}O-poor gas, resulted in the mass independent fractionation of oxygen isotope ratios among chondrules in CCs plotting along a slope ~1 line (e.g., Chaussidon et al. 2008; Schrader et al. 2013; 2014). The rates of the oxygen isotope exchange between the molten silicate and gas (H_2O) were experimentally determined by Yu et al. (1995) and Di Rocco and Pack (2015) in order to evaluate the degree of isotope exchange during a chondrule forming event using the appropriate oxygen fugacity (log fO_2 ~IW-4 to −2 for type I and IW-2 for type II chondrules; e.g., Zanda et al., 1994; Ebel and Grossman 2000). While 90% oxygen isotope exchange is achieved in 30 minutes at a log fO_2value 0.5 units below the IW buffer (experiments performed at 1 atm and 1450°C; Yu et al., 1995), only 50% of oxygen isotope exchange occurred at a lower log fO_2 (from IW-1.3 to IW-3.8) in 1–4 hours (experiments performed at 1 atm and 1500°C; Di Rocco and Pack, 2015). Based on the heating duration at temperatures above the liquidus predicted by the shock models (e.g., Desch and Connolly, 2002; Morris and Desch, 2010), Di Rocco and Pack (2015) estimated the degree of isotope exchange between the chondrule melt and ambient gas to be 50% and 70% for type I and type II chondrule formation conditions, respectively. Thus, the observed internal homogeneity among olivine and pyroxene phenocrysts in chondrules from this work and previous SIMS studies may not be explained unless chondrule precursor and ambient gas had similar Δ^{17}O values. Furthermore, the oxygen isotope homogeneity between olivine and mesostasis phases (e.g., high-Ca pyroxene, plagioclase, glass) reported from the most pristine chondrites such as Acfer 094 and CR chondrites (Ushikubo et al. 2012; Tenner et al. 2015) is hard to explain if the ambient gas and initial melt had distinct Δ^{17}O values, because continuous isotope exchange between melt and gas under liquidus temperatures (>10 h) would modify the oxygen isotope ratios of late forming minerals and quenched glass. In the case of chondrules in Murchison, we did not analyze plagioclase or glassy mesostasis that were altered during aqueous alteration. However, we analyzed high-Ca pyroxene grains in several chondrules that are indistinguishable from olivine and low-Ca pyroxene mesostasis in term of oxygen isotope ratios (Fig. 7). Chondrules in Murchison do not show internal oxygen isotope zoning with the crystallization sequence.

As discussed in previous studies (Kita et al. 2010; Ushikubo et al. 2012; Tenner et al. 2013; 2015; 2017), it is likely that the ambient gas during chondrule formation had oxygen isotope ratios close to those of solid precursors. Chondrules likely formed in dust-rich regions (enriched in CI dust by more than ~100×) of the protoplanetary disk (e.g., Ebel and Grossman, 2000; Ozawa and Nagahara, 2001; Alexander, 2004; Alexander et al., 2008; Nagahara et al., 2008; Schrader et al., 2013; Tenner et al., 2015) and in an open-system with significant evaporation and re-condensation (e.g., Cohen et al., 2004; Libourel et al., 2006; Nagahara et al., 2008; Hewins and Zanda, 2012). In consequences, the isotopic ratios of oxygen in the ambient gas would be controlled and dominated by those of the solid chondrules' precursors (Kita et al., 2010; Ushikubo et al., 2012). Recondensation of oxide further enhances the equilibration of the oxygen isotope ratios between the ambient gas and chondrule melt. Within this framework, the oxygen isotope ratios of the ambient gas and the melt would be similar to the averaged precursor solids that represent local disk regions.

In the series of SIMS oxygen isotope studies of chondrules in CR chondrites, Schrader et al. (2013; 2014) found that BO chondrules show systematically higher and narrower range of $\Delta^{17}O$ than porphyritic chondrule. The authors argued that the isotope exchange between the chondrule melt and ^{16}O-poor gas was incomplete for all cases, but higher in BO (~90%) than porphyritic chondrules (25–50%). In their model, the ambient gas formed during chondrule formation is derived from a ^{16}O-poor ice that was evaporated to a H_2O gas. While BO chondrules formed from complete melting and are individually homogeneous in term of oxygen isotope ratios, Schrader et al. (2014) suggested that the significant range of $\Delta^{17}O$ values observed for BO chondrules indicates that even BO chondrules did not experience complete isotope exchange. If true, we should see an isotope zoning in the mesostasis of porphyritic chondrules, in contrast to observations from previous works (e.g., Ushikubo et al. 2012; Tenner et al. 2015). Furthermore, systematically different ranges of $\Delta^{17}O$ values between BO chondrules and porphyritic chondrules in CR chondrites reported by Schrader et al. (2013; 2014) are actually fairly similar; from −3.8‰ to −1.3‰ and from −0.8‰ to +1.4‰ for type I and II BO chondrules, respectively, and from −4.6‰ to −0.3‰ and from −1.8‰ to +0.9‰ for type I and II porphyritic chondrules, respectively. By combining data from Tenner et al. (2015), the lower ends of type I BO chondrules and type I porphyritic chondrules extend to −5.3±0.4‰ and −5.9±0.2‰, respectively, which are marginally different. In the study of Allende chondrules by Rudraswami et al. (2011), the range of $\Delta^{17}O$ values are similar between type I BO and porphyritic chondrules; from −5.6‰ to 0‰ and from −5.8‰ to - 2.2‰, respectively. Alternatively, and as discussed above, a formation of chondrules in an open system and dust-rich environment suggests that oxygen isotope ratios of the chondrule melt and ambient gas would have been very similar and represent the average composition of the solid precursors of localized areas, including ice. As clearly observed, the difference between type I and II chondrules that formed under distinct oxygen fugacities indicates that each chondrite group collected chondrules formed in multiple environments with respect to oxygen isotope ratios. This scenario would explain the similar range of oxygen isotope ratios between BO chondrules and porphyritic chondrules observed in both CR and CV chondrites.

4.1.3. Isotope heterogeneity of chondrules with or without relict grains—Five chondrules were described as heterogeneous regarding the oxygen isotope ratios of their olivine and pyroxene grains (Table 2, Fig. 5). The precursors of these heterogeneous chondrules were thus less melted than the internally homogeneous chondrules. It suggests either a lower temperature of the melting event(s) or a shorter duration of melting, or both.

Interestingly, the four heterogeneous chondrules A7, B3, A8, and A4 have porphyritic textures (Table 2). Although chondrules A7 and A8 display more rounded shapes, the chondrules B3 and A4 have convoluted outlines and contain numerous metal (or altered metal) grains dispersed throughout fine-grained silicates (EA2). All these observations are consistent with an incomplete melting (e.g., Lofgren, 1996; Hewins and Radomsky, 1990; Zanda et al. 2002). Recent experimental works indicate fast dissolution rates of olivine (up to ~22 μm/min at 1531°C) during heating (Soulié et al., 2017). Because of the fast kinetics of dissolution of olivine in type I chondrule-like melts, the preservation of former olivine crystal in porphyritic chondrules required fast cooling rates, in the range of 1000–8000 K/h at 1500°C (Soulié et al., 2017). Although extended to higher cooling rates, these results are in agreement with those from experiments on mineral textures of type I porphyritic chondrules that reported values between 10 and 1000 K/h (e.g., Radomsky and Hewins, 1990; DeHart and Lofgren, 1996). The fifth heterogeneous chondrule displays a granular texture (C10; Fig. 2c). Granular textures also result from the incomplete melting of the precursor (initial temperature before cooling below the liquidus; Hewins and Radomsky, 1990). Both isotope ratios and textural observations support the fact that these five chondrules are internally heterogeneous in oxygen isotope ratios because of the low degree of melting of their isotopically heterogeneous solid precursors. Indeed, the ~50–90% melting experienced by such chondrules allows a high percent of former crystals to survive (e.g., Lofgren, 1996). It should be noted that the range of $\Delta^{17}O$ values in these chondrules significantly overlaps those defined by the host chondrule values (Fig. 5). This observation suggests common isotope reservoirs for the homogeneous chondrules and precursors of these heterogeneous ones.

Only two olivine grains from the heterogeneous chondrules A7 are significantly ^{16}O-rich ($\Delta^{17}O = -8.0$ and $-12.8‰$; Table 2, Fig. 5) compared to the other coexisting phases ($\Delta^{17}O$ from -4.6 to $-6.3‰$; Fig. 5) that are similar to the ^{16}O-rich relict olivine grains in homogeneous chondrules. Some of these ^{16}O-rich analyses could be caused by a small domain of AOA-like ^{16}O-rich olivine that might be present as relict grains within these chondrule phenocrysts (Nagashima et al., 2015). Especially, the most ^{16}O-rich data in A7 with $\Delta^{17}O$ of $-12.8\pm0.9‰$ show a large variability in $\delta^{18}O$ and $\delta^{17}O$ along a slope ~1 line within a single analysis. Such ^{16}O-rich domains could also occur as small μm-sized areas within other olivine analysis spots, which would result in lower $\delta^{17}O$ and $\delta^{18}O$ values along the PCM line compared to true host chondrule values. Although the changes are generally small and marginally resolvable beyond analytical uncertainties, we may not be able to completely rule out the possibility that some chondrules are recognized as “heterogeneous” due to frequent encounters with small ^{16}O-rich domains during SIMS analyses.

4.1.4. Abundance and origin of relict grains—One type II chondrule among the four analyzed in Murchison contains relict olivine grains (Fig. 5). Because of the small

number of type II chondrules analyzed, this abundance of 25% calculated may not be representative of the CM chondrites. Recently, Schrader and Davidson (2017) analyzed 84 type II chondrules in CM chondrites. Using the FeO content of olivine, these authors estimated that ~12% of type II chondrules in CM chondrites contain relict olivine grains. Whatever the method and the number of type II chondrules analyzed, these two values (12% and 25%) are significantly different that the abundance of ~48% of CO type II chondrules that contain relict grains (15/31; Jones, 1992; Wasson and Rubin, 2003; Kunihiro et al., 2004a; Tenner et al., 2013). As discussed by Schrader and Davidson (2017), this difference between CM and CO chondrites does not support a common parent body for these two groups of CCs.

For type I chondrules, approximately 40% of the chondrules investigated contain relict olivine grains, which are either ^{16}O-poor or ^{16}O-rich compared to the host chondrules (Fig. 5). The abundance of ~40% is very similar to those in Y-81020 (CO3.05; Tenner et al. 2013), Acfer 094 (ungroup C3.00; Ushikubo et al. 2012), and Kaba (CV3; Hertwig et al. 2018).

The presence of variable oxygen isotope ratios in a single chondrule can be interpreted as the consequence of the mixing process between ^{16}O-rich precursors and a ^{16}O-poor nebular gas (e.g., Krot et al., 2005). However, such model cannot explain the presence of ^{16}O-poor relict olivine grains (in chondrule A2) (Fig. 5). Although amoeboid olivine aggregates (AOAs) may have been the precursors of relict olivine grains with the lowest Δ^{17}O values (down to −17.9‰ in chondrule B6; Fig. 5), this result suggests that some relict olivine grains did not originated from AOA-like materials or ^{16}O-rich refractory precursors (e.g., Krot et al., 2006a, and references therein; Ushikubo et al., 2012). Twelve of the 19 relict olivine grains have Δ^{17}O values ranging between −3.4‰ and −6.0‰. They are thus possibly related to material formed in the major isotope reservoir (^{17}O~−5%) discussed above, as well as individual analyses from the five heterogeneous chondrules with Δ^{17}O values ranging between −4.0‰ and −6.5‰ (Table 2). It implies mixing events and material exchanges from one isotope reservoir to another at the time of chondrule formation, i.e., 2–4 Ma after CAIs (e.g., Kita and Ushikubo, 2012; Schrader et al., 2017a). Because approximately 35% of the chondrules investigated (both type I and type II) contain relict olivine grains and thus sampled at least two different oxygen isotope reservoirs, migration of chondrule and/or chondrule precursors within the protoplanetary disk may have been a common process.

The presence of relict olivine grains in some chondrules indicate that they did not completely melt during the heating event that formed the final liquids from which the pyroxene and the non-relict olivine grains crystallized. Due to the low diffusion coefficient of oxygen in olivine (~1×10^{-18} m/s^2 at 1700 K; Ryerson et al., 1989; Gerard and Jaoul, 1989, Dohmen et al., 2002), unmelted relict olivine grains can preserve their oxygen isotope signatures. A part of the relict grains could correspond to an earlier generation of chondrule olivine (e.g., Jones et al., 2004; Russell et al., 2005; Kita et al., 2010; Rudraswami et al., 2011; Ushikubo et al. 2012; Schrader et al., 2014; Tenner et al., 2015; Krot and Nagashima, 2017), though some of these relict olivine grains could originate from different disk regions (e.g., Berlin et al., 2011; Weisberg et al., 2011; Schrader and Davidson, 2017; Schrader et al., 2017b; Tenner et al. 2017). Furthermore, refractory precursors, such as AOA-like ^{16}O-

rich olivine, likely existed among chondrule precursors that survived chondrule melting, which suggest that some precursors would derive from oldest inner disk regions (e.g., MacPherson et al., 2012).

4.2. Mg# and oxygen isotope relationship: Implications for the Murchison chondrule formation

As previously expressed by Ushikubo et al. (2012) and Tenner et al. (2013; 2015; 2017), the detailed relationship between chondrule Mg#'s and their host oxygen isotope ratios at sub% precisions from a representative suite of chondrules (n≥30) can provide important information about the origin and formation of chondrules.

4.2.1. Chondrules with Mg# >98.5 and $\Delta^{17}O$ ~−5‰—As shown in Fig. 6, type I chondrules in Murchison become more ^{16}O-poor with decreasing Mg#, towards the $\Delta^{17}O$ values of type II chondrules at ~−2.5‰. With the exception of chondrule C6 ($\Delta^{17}O$: −1.2‰; Mg#: 99.6), chondrules with Mg#'s between 99.5 and 98.9 have $\Delta^{17}O$ values ranging from −6.0‰ to −4.1‰. These trends are similar to those obtained for type I chondrules in Acfer 094 and CO chondrites (Ushikubo et al., 2012; Tenner et al., 2013) (Fig. 8), and to a lesser extent for the Y-82094 ungrouped chondrite and CV chondrites (Libourel and Chaussidon, 2011; Rudraswami et al., 2011; Tenner et al., 2015, 2017; Hertwig et al., 2017; 2018; Kita et al., 2016). The majority of chondrules in CR and CH chondrites shows $\Delta^{17}O$ values higher than −4‰, while a small number of chondrules with $\Delta^{17}O$ = −5‰ and Mg#>98 has been reported (Nakashima et al. 2011; Schrader et al. 2013; 2014; Tenner et al. 2015). It indicates that all groups of CCs sampled a common Mg# ~99 chondrule-forming environment (e.g., same dust enrichment relative to the solar gas, similar H_2O content in solid precursors), with a $\Delta^{17}O$ ~−5‰.

This oxygen isotope reservoir, which can be found in each group of CC, was highly reducing. This is the same reservoir as the −5‰ oxygen isotope reservoir reported in previous works (e.g., Ushikubo et al., 2012) that is also called as the "−5.5‰" (Tenner et al., 2013) or the −5‰ ± 1‰ reservoir (Tenner et al., 2017). Based on thermodynamic equilibrium calculations (e.g., Ebel and Grossman 2000), Mg#'s of ~99 indicate formation at low fO_2 ~−3.5 log units below the IW buffer (e.g., Tenner et al., 2015). As shown in Fig. 6, $\Delta^{17}O$ values increase as chondrule Mg#'s decrease from 99.5. Similar to those in CR chondrite chondrules (Tenner et al. 2015), this relationship can suggest an addition of ^{16}O-poor H2O ice to the nearly anhydrous chondrule precursors, to form more oxidized chondrules with higher $\Delta^{17}O$ values and lower Mg#'s. According to the mass balance calculations involving a ^{16}O-rich anhydrous dust and ^{16}O-poor H2O ice that were given in Tenner et al. (2015) to model Mg#-$\Delta^{17}O$ diagram of CR chondrite chondrules, Mg# 99 chondrules with a similar $\Delta^{17}O$ values in Murchsion might form at dust to gas ratios of ~50× of solar gas and from dust with 0–0.4× the atomic abundance of H2O ice, relative to CI dust. In addition to this mixing process, an increase of the dust to gas ratios can also be invoked for formation of more oxidized chondrules, as well as a combination of these two processes.

We can also note here that one POP chondrule (C6) in Murchison has a high Mg# (99.6) but a higher $\Delta^{17}O$ (−1.2%) that differs from the trend defined by chondrules with Mg#'s > 98.5

(Fig. 6). One type I PP chondrule containing dusty olivine grains in Acfer 094 and one BO chondrule in Y-81020 also display $\Delta^{17}O$ values ranging between −3.3% and −1.2% for Mg# >98.5 (Fig. 8). There are no textural or chemical similarities among these three chondrules.

4.2.2. Chondrules with Mg# <96 and $\Delta^{17}O$ ~−2.5‰—The four type II chondrules analyzed and the type I GOP chondrule C8 have host $\Delta^{17}O$ values of around −2.5% (−2.7±0.3‰ to −2.3±0.2‰) for Mg#'s ranging from 64.9 to 96.0 (Table 1, Fig. 6). These characteristics were reported for many chondrules from Acfer 094 (Ushikubo et al., 2012), the Y-81020 CO3.0 chondrite (Tenner et al., 2013) (Fig. 8), as well as from the Y-82094 ungrouped chondrite (Tenner et al., 2017). Some chondrules in CR (Schrader et al., 2013, 2014; Tenner et al., 2015) and a few in CV3 oxidized (Rudraswami et al., 2011; Hertwig et al., 2018) chondrites also display these characteristics. These observations suggest that in addition to the $\Delta^{17}O$ ~−5% reservoir, another oxygen reservoir ($\Delta^{17}O$ ~−2.5‰) may have been ubiquitous in the region of the protoplanetary disk where CCs formed. However, chondrules in CCs are predominantly type I (Jones, 2012). As noticed by Tenner et al. (2015; 2017), the low modal abundance of type II chondrules relative to type I chondrules in CCs (e.g., Zanda et al., 2006, Jones, points out a probable limited chondrule-forming region for type II chondrules, in term of time and/or volume.

The increase of the oxidation state required by the formation of type II chondrules is often associated with an enhancement of the dust/gas ratios (Ebel and Grossman, 2000; Fedkin and Grossman, 2016) and ice contents in the chondrule precursors (e.g., Fedkin and Grossman, 2006). According to Tenner et al. (2015), the dust to gas ratio may have been variable (~300–2000× solar composition) to account for the range of oxygen fugacities required to form these chondrules (Mg#'s ranging from 65 to 96). Regarding predictions from dynamic models of the protoplanetary disk (e.g., Cuzzi et al., 2001), these high dust enrichments (up to ~2000×) were relatively rare. Thus, it may be the cause of the predominance of type I chondrules compared to type II chondrules in CM chondrites, as in Acfer 094 and Y-81020. Indeed, approximately 20% of chondrules in Acfer 094 are type II (Kunihiro et al., 2005), ~10% and ~10–40% in CO and CM, respectively (Jones, 2012). In Murchison, we only found 10 type II chondrules (excluding fragments and isolated Fe-rich olivine grains) among a total of around 150 chondrules initially identified from three thin sections, suggesting that the abundance of type II chondrules might be lower than 10%, an abundance closer to the value reported for CV chondrites ~5% of chondrules are type II; Jones, 2012).

Interestingly, the type I chondrules with Mg#'s of ~94–96 in CM, CO, and Acfer 094 have host $\Delta^{17}O$ values of ~−2.5‰ (Fig. 8). This ~−2.5‰ value is characteristic of the type II chondrules in CM, CO, and Acfer 094 (Fig. 8). These chondrules have not been observed in CR and CV3 chondrites, in which less than 5% of chondrules are type II. In CR chondrites, some type I chondrules have Mg# ranging between 90 and 96 but their host $\Delta^{17}O$ values are dispersed around ~−3.5‰ and ~−1‰ (Schrader et al., 2013, 2017a; Tenner et al. 2015). Although the $\Delta^{17}O$ ~−2.5‰ isotope reservoir in CM, CO and Acfer 094 is extended towards high Mg# values (up to 96) compared to CV and CR chondrites, it does not seem to support a continuous trend between Mg#'s ~99 and ~65. Compared to chondrules with Mg# > 98.5 (see section 4.2.1), the relatively constant $\Delta^{17}O$ values observed here over a wide range of

lower Mg#'s suggest an existence of homogenized isotope reservoirs. Such reservoirs could have been formed as a result of the mixing between ^{16}O-rich anhydrous dust and ^{16}O-poor water ice, as in the case of model endmembers by Tenner et al. (2015) with Δ^{17}O values of −6‰ and +5‰, respectively.

4.3. The CO-CM relationship

4.3.1. Chondrules in CO, and CM chondrites—In order to investigate the possible CO-CM relationship, we compared our oxygen isotope data obtained for Murchison to those from the CO3.0 chondrite Y-81020, as well as Acfer 094, which can be considered similar to the primitive CM material before aqueous alteration (e.g., Rubin et al., 2007; Hewins et al., 2014) (Fig. 8). Many chondrules from Murchison, Acfer 094, and Y-81020 have Mg#'s higher than 98, with Δ^{17}O values ranging between approximately −6‰ and −4‰ (Fig. 8). These CCs sampled a same highly reduced and ^{16}O-rich reservoir (see also section 4.2.1). They also sampled a common ^{16}O-poor reservoir with Δ^{17}O values of around −2.5‰, corresponding to chondrules with Mg#'s lower than ~96. As Y-81020, it appears that Murchison did not sample the reservoir observed in CR chondrites and characterized by Δ^{17}O values of 0% and Mg#'s < 96 (Connolly and Huss, 2010; Schrader et al., 2013, 2014, 2017a; Tenner et al., 2015). The bimodal distribution of the Δ^{17}O values and the Δ^{17}O-Mg# relationship observed in chondrules from Murchison is thus similar to those observed in the Y-81020 CO3.0 chondrite by Tenner et al. (2013). Another similarity between Murchison, Y-81020, and Acfer 094, is the apparent lack of chondrules with Δ^{17}O ~−4‰ to ~−1‰ and Mg#'s of 98.5–97. Recent studies also indicate that this same component is absent in chondrules from CV chondrites (Hertwig et al., 2017; 2018). In contrast, these type I chondrules were commonly observed in CR chondrites (Schrader et al., 2013, 2014, Tenner et al., 2015).

In terms of both Mg#'s and oxygen isotope ratios, our data thus confirm that CM and CO chondrites contain a similar and indistinguishable population of chondrule. It thus supports a common origin for chondrules from these both groups of CCs. This result is in agreement with the chemical similarities reported by Frank et al. (2014) and Schrader and Davidson (2017) for the high-temperature anhydrous silicates in CO and CM chondrites.

As shown in Fig. 9, type II chondrule olivines in Murchison display the same MnO-FeO correlation as other CM chondrites (Frank et al., 2014; and references therein) including the Paris CM2 chondrite (Hewins et al., 2014; without chondrule #3). This correlation is also similar to that for CO chondrites (Berlin et al., 2011; Jones, 2012; Tenner et al., 2013; Schrader and Davidson, 2017) and Acfer 094 (Frank et al., 2014; Ushikubo et al., 2012) (Fig. 9), but is different from what has been observed for OCs and CR chondrites (Berlin et al., 2011; Schrader et al., 2015; Schrader and Davidson, 2017). As discussed by Schrader and Davidson (2017), this similar FeO/MnO correlation in olivine from CO and CM chondrules indicates similar formation conditions (e.g., oxygen fugacity, chondrule precursor compositions). According to data from this study, Ushikubo et al. (2012), and Tenner et al. (2013), type II chondrules in CM, CO, and Acfer 094 have similar FeO/MnO ratios of olivine (~100), similar ranges of Mg#'s (<96), and similar oxygen isotope ratios

($\Delta^{17}O$ ~−2.5‰), which reflects a common formation environment. These data further strengthen the existence of the CO-CM genetic link.

Many olivine grains in type II chondrules from reduced CV chondrites also displays FeO and MnO values that partially overlap the CO-CM field (Frank et al., 2014). In comparison, type II chondrules from oxidized CV chondrites have FeO and MnO contents closer to those measured in olivine in type II chondrules in OCs (Frank et al., 2014; and references therein) and CR chondrites (Berlin et al., 2011; Frank et al., 2014; Schrader et al., 2015). Acfer 094, CO, and CM chondrules thus shared similar formation conditions with at least some CV chondrules, suggesting a common environment in the same region of accretion. Regarding the relative low abundance of type II chondrules in the different groups of CCs compared to type I chondrules (e.g., Scott and Taylor, 1983; Jones, 1992; Weisberg et al., 1993; Kunihiro et al., 2005), this common environment was likely localized in the protoplanetary disk where CCs accreted.

The relict olivine grains from the Murchison and Paris (Hewins et al., 2014) chondrules plot within the fields defined by type I and type II chondrules and some within the gap between them (Fig. 9). As also indicated from oxygen isotope systematics of Murchison chondrules, this observation supports that mechanical exchanges occurred between the type I and type II chondrule-forming reservoirs. Ushikubo et al. (2012) also reported that most of the relict grains in Acfer 094 have $\Delta^{17}O$ values corresponding to the two major reservoirs discussed above ($\Delta^{17}O$: −5‰; $\Delta^{17}O$: −2.5‰). Migration of solid precursor may have occurred between these two isotope reservoirs, suggesting they both existed in the protoplanetary disk at the time of chondrule formation (e.g., Ushikubo et al., 2012). Although their spatial relationships are still not known, materials from these $\Delta^{17}O$ "−5‰" and "−2.5‰" reservoirs may have been contemporaneous and near each other (Kurahashi et al., 2008; Tenner et al., 2013; Ushikubo et al., 2013). This oxygen isotope relationship between type I and type II chondrules is in good agreement with petrological and chemical observations. For example, type I forsterite and metal relict grains were reported in type II chondrules in CR, CO, and LL ordinary chondrites (Wasson and Rubin, 2003; Ruzicka et al., 2007; Schrader et al., 2008). Type II chondrules could have been formed from the oxidation of type I chondrules (Connolly et al., 2008; Schrader et al., 2008; Ruzicka et al., 2008; Connolly and Huss, 2010), although a compositionally similar precursor for type I and type II cannot be definitely ruled out. Recently, Villeneuve et al. (2015) experimentally investigated the origin of type II chondrules. The authors also concluded that type II chondrules were mainly formed from type I chondrule material under oxidizing conditions, as supported by the occurrence of fayalitic olivine grains with relict forsterite cores (e.g., Wasson and Rubin, 2003; Ruzicka et al., 2007).

4.3.2. Whole rock and other chondritic components in CO and CM chondrites—

The high temperature components in CM and CO chondrites are indistinguishable in term of $\Delta^{17}O$-Mg# relationship and oxygen isotope ratios. The average oxygen isotope ratios of type I chondrules in Murchison with Mg# > 98.5 and $\Delta^{17}O$ ~−5‰ (except for chondrule C6) is −3.9‰ and −7.1% for $\delta^{18}O$ and $\delta^{17}O$, respectively. The oxygen isotope ratios of type I chondrules with Mg# > 98.5 and $\Delta^{17}O$ ~−5‰ in the Y-81020 CO3 chondrite ($\delta^{18}O$: −5.8‰; $\delta^{17}O$: −8.6‰) are very similar to those measured for type I

chondrules in Murchison (Fig. 10). In the same way, the average oxygen isotope ratios of type II chondrules in Murchison is 2.5‰ and −1.1‰ for $\delta^{18}O$ and $\delta^{17}O$, respectively (Fig. 10). These values are also very close to those of the average oxygen isotope ratios of type II chondrules in the Y-81020 CO3.0 chondrite that are −2.0‰ and −1.4‰ for $\delta^{18}O$ and $\delta^{17}O$, respectively (Fig. 10).

The average oxygen isotope ratios of type I chondrules in Murchison are very close to those measured by Clayton and Mayeda (1984) (−4.2‰ and −7.4‰ for $\delta^{18}O$ and $\delta^{17}O$, respectively) for the anhydrous mineral separates from Murchison. In term of oxygen isotope ratios, type I chondrules can thus be considered as representative of the anhydrous part of CM chondrites, as it was calculated for Murchison from seven fractions of olivine +pyroxene with density >3.18 obtained using a density separation method (Clayton and Mayeda, 1984). It is consistent with low abundance of type II chondrules in CM chondrites, possibly less than 10% of the whole chondrule population in Murchison as described earlier. Thus, type II chondrules with higher $\delta^{18}O$ and $\delta^{17}O$ values do not significantly contribute to the oxygen isotope ratios of the anhydrous part of CM chondrites, or are balanced by a small contribution from ^{16}O-rich refractory inclusions in CM chondrites (e.g., Brearley and Jones, 1998; and reference therein).

As initially proposed by Clayton and Mayeda (1999) and later observed within a single whole rock (the Paris CM2 chondrite; Hewins et al., 2014), CM2 chondrites can be considered in term of oxygen isotope ratios as a mixture of two components between ^{16}O-rich anhydrous silicates (represented by type I chondrules) and ^{16}O-poor hydrated phases (matrix). This two component mixing is clearly seen in Fig. 10 in which the average value of type I chondrules in CM plots along the CM mixing line that also pass through the field defined by the bulk compositions of the CO falls (Fig. 10). Regarding our results, it seems that the genetic CO-CM link previously suggested on the basis of their oxygen isotope ratios was due to the similarity between oxygen isotope ratios of anhydrous components of CM and those of bulk CO chondrites. Because of limited degrees of aqueous alterations and thermal metamorphism in CO chondrites, bulk CO chondrites show a narrow range of oxygen isotope ratios, which remained close to those of their ^{16}O-rich anhydrous components. Indeed, CO chondrites are also dominated by type I chondrules (e.g., Jones, 2012), so that their bulk compositions are very similar to the average compositions of type I chondrules (Fig. 10). By comparison, bulk compositions of CV chondrites display more variability along the CCAM line because of secondary alteration processes (e.g., Clayton and Mayeda, 1999), while pristine type I chondrules in CV chondrites display similarities with type I chondrules from both CM and CO chondrites (Hertwig et al., 2017; 2018). This study thus highlighted the fact that CM chondrites contain high temperature components very similar to other major CCs, not only CO chondrites. The isotope signatures of such components are well preserved in chondrule mafic minerals in Murchison, while bulk Murchison contains a significant amount of low temperature components, such as organic matter, hydrated chondrule mesostasis, and matrix phases.

4.3.3 A single CO-CMparent body?—As discussed above, CM and CO chondrules are similar in terms of oxygen isotope systematics (Tenner et al., 2013; Chaumard et al., 2016; Schrader et al., 2017b) and major and minor element compositions (e.g., Berlin et al.,

2011; Schrader and Davidson, 2017). In addition, it has been shown that CO and CM chondrites display similar refractory lithophile element abundances (Kallemeyn and Wasson, 1981). Oxygen isotope studies of bulk CM and CO chondrites show characteristic relationships indicating their genetic relationships (Fig. 10). It has been argued that similar observed properties of CO and CM chondrites may indicate they originated from a single parent body. However, CO chondrites are less hydrated than CM chondrites (e.g., Keller and Buseck, 1990), suggesting that the abundance of water/ice accreted with both chondrites were quite different. As discussed by Greenwood et al. (2014), a possible explanation for water/ice abundances is that CO and CM chondrites might sample the dehydrated inner part and hydrated surface of a single parent body, in which aqueous fluids were generated in the inner part and moved outwards during the heating of the parent body (Fu and Elkins-Tanton, 2014). However, this scenario may not explain the compositional gap in oxygen isotope ratios between the fields defined by the bulk CM and CO falls (Fig. 10), which were recently reduced from the Paris data (Hewins et al., 2014).

Alternatively, CM and CO chondrites may thus derive from two different parent bodies that accreted similar ^{16}O-rich high temperature and anhydrous components but with different amount of ice/water. Although some CO3 chondrites experienced limited hydrothermal alteration (e.g., Rubin, 1998), i.e., producing secondary magnetite and fayalite (e.g., Doyle et al., 2015), the CO parent body was significantly less hydrated than the CM parent body. This is supported by the observation of many CO3 chondrites with low degrees of thermal metamorphism that still display pristine features such as the presence of Si and Fe-rich amorphous silicate material (i.e., in the CO3.0 Allan Hills A77307; Brearley 1993) and metal (e.g., Keller and Buseck, 1990).

Several properties of CO and CM chondrites argue against a common parent body. There are differences in the chondrule sizes (0.15 and 0.30 mm in CO and CM chondrites, respectively; e.g., Rubin and Wasson, 1986; Rubin, 1989, 2010; May et al., 1999; Weisberg et al., 2006; Friedrich et al., 2015; Schrader and Davidson, 2017), abundance of matrix (30–35 and 70 vol.% in CO and CM chondrites, respectively; Scott et al., 1996; Weisberg et al., 2006; and references therein), cosmic-ray exposure ages (Eugster, 2003), bulk compositions of chondrules from CO and CM chondrites (Rubin and Wasson, 1986), and abundance of FeO-poor relict grains in type II chondrules (see section 4.3; Schrader and Davidson, 2017). Furthermore, lack of breccias composed of CO- and CM-like materials is another argument against a common parent body (Bischoff et al., 2006). As also discussed by Schrader and Davidson (2017), the relationship between the bulk oxygen isotope (Greenwood et al., 2014) and ε^{54}Cr compositions (Sanborn et al., 2015) of CO and CM chondrites may not support a common origin from a single parent body.

4.3.4. Accretion time and location relative to the snow line—Constraints on the accretion times of the CO and CM parent bodies were recently provided by the study of their peak temperatures and Mn-Cr ages of aqueously-formed phases. Based on secondary fayalite, Doyle et al. (2015) reported an accretion time of the CO parent body of ~2.1–2.4 Ma after CAI formation. Fujiya et al. (2012) studied secondary calcite and dolomite in the CM chondrites Murchison, Y-791198, Allan Hills 83100, and Sayama. In order to compare results from CO and CM chondrites, Doyle et al. (2015) recalculated the relative ages of CM

chondrites analyzed by Fujiya et al.(2012). These corrected ages recalculated by Doyle et al. (2015) and anchored to the same U-corrected Pb-Pb age of the D'Orbigny angrite and relative to the age of CV CAIs give an accretion time of the CM parent body of ~3.7–5.0 Ma after CAIs. Although they use a different CAI age, Sugiura and Fujiya (2014) also calculated a late age of accretion of the CM parent body (~3.5 Ma) by comparison to the CO parent body (~2.7 Ma).

^{26}Al-^{26}Mg systematics of chondrules from the Y-81020 CO3.05 chondrite indicate of formation of type I and type II chondrules 1.7–2.5 and 2.0–3.0 Ma after CAI formation, respectively (Kunihiro et al. 2004b; Kurahashi et al., 2008). Formation ages of type I chondrules are fully consistent with the accretion time of CO3, while type II seem to have been formed slightly later, nearly 1 Ma after the estimated accretion time. The metamorphic temperatures of Y-81020 has been estimated to be 400–550°C using metal chemistry (Shibata and Matsueda 1994; Kimura et al. 2008). At this temperature range, some type II chondrules in Y-81020 may have been disturbed in their Al-Mg system due to fast Mg diffusion in Na-rich plagioclase that commonly occur among type II chondrules (Van Orman et al. 2014). Because of intense secondary processes, formation ages of chondrules in CM chondrites cannot be resolved yet.

Regarding their chemical properties, it is commonly considered that CCs derived from parent bodies formed in the protoplanetary disk at different times and/or locations, as well as various ice/water and dust contents (e.g., Zolensky and McSween, 1988; Brealey, 2006; Chambers, 2006; Krot et al., 2006b; and references therein). With a low water ice/rock mass ratio (~0.1–0.2; Doyle et al., 2015), CO chondrites might be accreted very close to the snow line (e.g., Wood et al, 2005), where the evaporation of ice was not efficient enough to destroy ice-rich particles (e.g., Cyr et al., 1998; Lunine, 2006). Contrary to CO chondrites, CM chondrites have larger water ice/rock mass ratios (~0.3–0.6; Clayton and Mayeda, 1999). It implies that the CM parent body formed beyond the snow line.

Depending on many parameters such as the luminosity of the proto-Sun, the opacity of the disk, and the mass transport throughout the protoplanetary disk, the location of the snow line likely varied with time (e.g., Ciesla and Cuzzi, 2006; Min et al., 2011; Oka et al., 2011; Martin and Livio, 2012; Cieza et al., 2016). As discussed by Doyle et al. (2015), the snow line may have been located around 2–3 AU at the formation of the CO parent body, implying an accretion in the inner part of the Solar System, i.e., close to the current position of the asteroid belt. Because CM and CO chondrites both sampled the same high-temperature ^{16}O-rich components, it would imply they accreted at the same location across the protoplanetary disk. Indeed, the snow line can move towards the Sun during the early evolution of the disk (e.g., Ciesla and Cuzzi, 2006; Min et al., 2011;Martin and Livio, 2012). Thus, the snow line would have been situated near the 2–3 AU region of the disk when the CO parent body formed (~2.1–2.4 Ma after CAI formation; Doyle et al., 2015), then closer to the Sun at the accretion time of the CM parent body (~3.7–5.0 Ma after CAI formation; ages from Fujiya et al., 2012 corrected by Doyle et al., 2015) that accreted more ice/water than CO chondrites. Within this framework, chondrules in CM could have been formed at the same time as those from CO chondrites, or later. Unfortunately, and as mentioned above, there is no formation ages of CM chondrules because the Al-rich phases in mesostasis are altered and not suitable

for ^{26}Al-^{26}Mg chronometers, nor U-Pb and other chronometers. Bouvier et al. (2013) reported bulk Mg isotope measurements of a series of chondrules from the Murchison and Murray CM2 chondrites. No detectable ^{26}Mg* variations was measured in all the chondrules analyzed, even for the one with the highest ^{27}Al/^{24}Mg ratio (though only 0.316; Bouvier et al. 2013). The authors concluded that CM chondrules were formed >1 Ma after CAIs, or more possibly, that the Al-Mg isotope systematics were reset by secondary parent body alteration processes after the decay of ^{26}Al. Although there are numerous similarities between the high-temperature components of chondrules in CO and CM chondrites, we thus cannot argue for a simultaneous formation.

CM-like clasts are ubiquitous within impact breccias of other groups/classes of meteorites (e.g., Zolensky et al., 1996; Gounelle et al., 2003; Bischoff et al., 2006; and references therein) and suggests that CM-like material was widespread in the early Solar System. Although most of the CM2 chondrites likely originated from a parent body in near Earth orbit (Morbidelli et al., 2006), it may support the existence of additional CM parent bodies (e.g., Zolensky et al., 1996). Our data cannot rule out the possibility of multiple CM parent bodies accreted beyond the snow line. However, and as discussed by Hewins et al. (2014), it may be unlikely that CM2 chondrites derived from different parent bodies while they experienced very similar aqueous alteration processes.

5. CONCLUSIONS

The main conclusions obtained by the *in-situ* oxygen three-isotope analyses of olivine and pyroxene grains in chondrules from the Murchison CM2 chondrite are:

1. Most chondrules consist of olivine grains with oxygen isotope ratios similar to coexisting pyroxene grains suggesting a co-magmatic crystallization. The host values calculated for these internally homogeneous chondrules are considered as representative of the final melt from which olivine and pyroxene crystallized.
2. Some olivine grains in chondrules were considered as relict grains with distict oxygen isotope ratios, which formed earlier than the coexisting minerals and survived during the high-temperature event of the final melt. Since most of the relict olivine grains have oxygen isotope ratios within the range defined by the host chondrule values (Δ^{17}O from ~−2% to ~−6%), multiple mixing events and material exchanges likely occurred at the time of chondrule formation.
3. Based on the variations of the oxygen isotope ratios of their coexisting olivine and pyroxene grains, five chondrules were described as heterogeneous in oxygen isotope ratios. As supported by their textures, these heterogeneous chondrules might result from the incomplete melting of former chondrule precursors because of a lower degree of the melting event and/or a shorter duration of melting.
4. Oxygen isotope ratios of host chondrules plot close to the PCM line, with Δ^{17}O values ranging from −6.0‰ to −1.2‰. With one exception, chondrules with high Mg# (>98.5) have host Δ^{17}O values of~−5‰ consistent with a formation in a reducing environment and dust to gas ratios of ~50×. Chondrules with lower

Mg# (~96–65) have host $\Delta^{17}O$ values of ~−2.5‰. These characteristics are consistent with a formation at high dust to gas ratios (up to ~2000×), from the anhydrous precursor of $\Delta^{17}O$ ~ −5‰ that formed Mg# ~99 chondrules, enriched in H2O ice (~0.3–0.4× the CI dust; Tenner et al., 2015). These two reservoirs are similar to those also sampled by other CCs, such as CV (Libourel and Chaussidon, 2011; Rudraswami et al., 2011; Hertwig et al., 2017; 2018), CO (Tenner et al., 2013), Y-82094 (Tenner et al., 2017), and Acfer 094 (Ushikubo et al., 2012).

5. In term of both Mg# and oxygen isotope ratios, the populations of chondrules sampled by CM and CO chondrites are indistinguishable. CO and CM chondrites thus contain similar high-temperature anhydrous silicates, as also supported by the Fe/Mn ratios of the olivine grains in type II chondrules from these two groups of CCs and reduced CV chondrites (Berlin et al., 2011; Tenner et al., 2013; Frank et al., 2014; Hewins et al., 2014; Scharder and Davidson, 2017).

6. Based on chondrule oxygen isotope systematics, we further argued that CM and CO chondrites might derive from distinct parent bodies with different amount of water/ice but accreted similar high-temperature ^{16}O-rich components, rather than a common parent body. The difference in water/ice abundance between the CO and CM parent bodies might be related to the location of the snow line compared to their accretion regions. The snow line probably moved through the CO and CM chondrule-forming regions towards the Sun between the accretion time of the CO and CM parent bodies, which are considered to be ~2.1–2.4 and ~3.7–5.0 Ma after CAI (Fujiya et al., 2012; Doyle et al., 2015), respectively.

Supplementary Material

Refer to Web version on PubMed Central for supplementary material.

ACKNOWLEDGEMENTS

We gratefully thank Glenn MacPherson (Smithsonian Institution) for selecting and allocating us Murchison thin sections suitable for the SIMS work. We are indebted to Andreas Hertwig and Travis Tenner for enlightening discussions. We thank John Fournelle and Jim Kern for assistance with electron probe micro-analysis and SIMS instrument, respectively. We are very grateful to Kazuhide Nagashima, Devin L. Schrader, and the AE, Sarah S. Russell, as well as an anonymous reviewer for their very constructive reviews and helpful comments, which led to major improvements to this manuscript. This work is supported by the NASA Cosmochemistry program (NNX14AG29G). WiscSIMS is partly supported by NSF (EAR13–55590).

REFERENCES

Alexander CMO'D (2004) Chemical equilibrium and kinetic constraints for chondrule and CAI formation conditions. Geochim. Cosmochim. Acta 68, 3943–3969.

Alexander CMO'D, Grossman JN, Ebel DS, and Ciesla FJ (2008) The formation conditions of chondrules and chondrites. Science 320, 1617–1619. [PubMed: 18566282]

Anders E and Grevesse N (1989) Abundances of the elements: meteoritic and solar. Geochim. Cosmochim. Acta 53, 197–214.

Baertschi P (1976) Absolute ^{18}O content of standard mean ocean water. Earth Planet. Sci. Lett 31, 341–344.

Benedix GK, Leshin LA, Farquhar J, Jackson T, and Thiemens MH (2003) Carbonates in CM2 chondrites: Constraints on alteration conditions from oxygen isotopic compositions and petrographic observations. Geochim. Cosmochim. Acta 67, 1577–1588.

Berlin J, Jones RH, and Brearley AJ (2011) Fe-Mn systematics of type IIA chondrules in unequilibrated CO, CR, and ordinary chondrites. Meteor. Planet. Sci 45, 513–533.

Bischoff A, Scott ERD, Metzler K, and Goodrich CA 2006 Nature and origins of meteoritic breccias In Meteorites and the early solar system II, edited by Lauretta DS and McSween HY, Jr. Tucson, Arizona: The University of Arizona Press pp. 679–712.

Bouvier A, Wadhwa M, Simon SB, and Grossman L (2013) Magnesium isotopic fractionation in chondrules from the Murchison and Murray CM2 carbonaceous chondrites. Meteorit. Planet. Sci 48, 339–353.

Brearley AJ (1993) Matrix and fine-grained rims in the unequilibrated CO3 chondrite, ALH A77307: Origins and evidence for diverse, primitive nebular dust components. Geochim. Cosmochim. Acta 57, 1521–1550.

Brearley AJ (2003) Nebular versus parent-body processing In Meteorites, comets, and planets., edited by Holland HD and Turekian KK Treatise on Geochemistry, vol. 1 Oxford: Elsevier-Pergamon pp. 247– 268.

Brearley AJ and Jones RH (1998) Chondritic meteorites In Planetary Materials, edited by Papike JJ Reviews in Mineralogy, vol. 36 Washington, D.C.: Mineralogical Society of America pp. 3-1–3-398.

Browning L, McSween HY, and Zolensky ME (1996) Correlated alteration effects in CM carbonaceous chondrites. Geochim. Cosmochim. Acta 60, 2621–2633.

Busemann H, Alexander CMO'D, and Nittler LR (2007) Characterization of insoluble organic matter in primitive meteorites by microRaman spectroscopy. Meteor. Planet. Sci 42, 1387–1416.

Chakraborty S (2010) Diffusion coefficients in olivine, wadsleyite, and ringwoodite In Reviews in Mineralogy and Geochemistry, 72 (eds. Zhang Y and Cherniak DJ). Mineralogical Society of America, Washington, DC, pp. 603–639.

Chambers J (2006) Meteoritic diversity and planetesimal formation In Meteorites and the Early Solar System II, edited by Lauretta DS and McSween HY, Jr. Tucson, Arizona: University of Arizona Press pp. 487–497.

Chaumard N Defouilloy C, and Kita NT (2016) Oxygen isotopes in chondrules from the Murchison CM2 chondrite and evidence for a CO-CM link. In 79th Annual Meteoritical Society Meeting, p. #6408, abstr.

Chaumard N, Hertwig AT, Kita NT, Tenner TJ, and Kimura M (2017) Measurements of silica excess in plagioclase in chondrules from primitive carbonaceous chondrites: Implications for 26Al-26Mg systematics. In 80h Annual Meteoritical Society Meeting, p. #6309, abstr.

Chaussidon M, Libourel G, and Krot AN (2008) Oxygen isotopic constraints on the origin of magnesian chondrules and on the gaseous reservoirs in the early Solar System. Geochim. Cosmochim. Acta 72, 1924–1938.

Ciesla FJ and Cuzzi JN (2006) The evolution of the water distribution in a viscous protoplanetary disk. Icarus 181, 178–204.

Cieza LA, Casassus S, Tobin J, Bos SP, Williams JP, Perez S, Zhu Z, Caceres C, Canovas H, Dunham MM, Hales A, Prieto JL, Principe DA, Schreiber MR, Ruiz-Rodriguez D, and Zurlo A (2016) Imaging the water snow-line during protostellar outburst. Nature 535, 258–261. [PubMed: 27411631]

Clayton RN, Onuma N, Grossman L, and Mayeda TK (1977) Distribution of presolar component in Allende and other carbonaceous chondrites. Earth Planet. Sci. Lett 34, 209–224.

Clayton RN and Mayeda TK (1984) The oxygen isotope record in Murchison and other carbonaceous chondrites. Earth Planet. Sci. Lett 67, 151–166.

Clayton RN and Mayeda TK (1999) Oxygen isotope studies of carbonaceous chondrites. Geochim. Cosmochim. Acta 63, 2089–2104.

Clayton RN, Onuma N, Ikeda Y, Mayeda TK, Hutcheon ID, Olsen EJ, and Molini-Velsko C (1983) Oxygen isotopic compositions of chondrules in Allende and ordinary chondrules. In Chondrules and their Origins, edited by Kring EA. Lunar and Planetary Institute, pp. 37–43.

Cohen BA, Hewins RG, Alexander CMO (2004) The formation of chondrules by open-system melting of nebular condensates. Geochim. Cosmochim. Acta 68, 1661–1675.

Connolly HC, Jr. and Huss GR (2010) Compositional evolution of the protoplanetary disk: oxygen isotopes of type-II chondrules from CR2 chondrites. Geochim. Cosmochim. Acta 74, 2473–2483.

Connolly HC, Jr., Huss GR, Nagashima K, Weisberg MK, Ash RD, Ebel DS, Schrader DL, and Lauretta DS (2008) Oxygen isotopes and the nature and origins of type-II chondrules in CR2 chondrites. In 39th Lunar and Planet. Sci. Conf. CD-ROM, p. #1675, abstr.

Cuzzi SJ, Hogan RC, Paque JM, and Dobrovolskis AR (2001) Size-selective concentration of chondrules and other small particles in protoplanetary nebula turbulence. Astrophys. J 546, 496–508.

Cyr KE, Sears WD, and Lunine JI (1998) Distribution and evolution of water ice in solar nebula: Implications for solar system body formation. Icarus 135, 537–548.

DeHart JM and Lofgren GE (1996) Experimental studies of group A1 chondrules. Geochimica et Cosmochimica Acta 60, 2233–2242.

Desch SJ and Connolly HC, Jr. 2002 A model of thermal processing of particles in solar nebula shocks: Application to the cooling rates of chondrules. Meteor. Planet. Sci 37, 183–207.

Dohmen R, Chakraborty S, and Becker HW (2002) Si and O diffusion in olivine and implications for characterizing plastic flow in the mantle. Geophys. Res. Lett 29 (21), 26-1–26-4

Doyle PM, Jogo K, Nagashima K, Krot AN, Wakita S, Ciesla FJ, and Hutcheon ID (2015) Early aqueous activity on the ordinary and carbonaceous chondrite parent bodies recorded by fayalite. Nature Communications 6, 7444.

Di Rocco T and Pack A (2015) Triple oxygen exchange between chondrule melt and water vapor: an experimental study. Geochim. Cosmochim. Acta 164, 17–34.

Ebel DD and Grossman L (2000) Condensation in dust-enriched systems. Geochim. Cosmochim. Acta 64, 339–366.

Eugster O (2003) Cosmic-ray exposure ages of meteorites and Lunar rocks and their significance. Chem. Erde 63, 3–30.

Fedkin AV and Grossman L (2006) The fayalite content of chondritic olivine: Obstacle to understanding the condensation of rocky material In Meteorites and the Early Solar System II (eds. Lauretta DS and McSween HY). University of Arizona Press, Tucson, Arizona, pp. 279–294.

Fedkin AV and Grossman L (2016) Effects of dust enrichment on oxygen fugacity of cosmic gases. Meteorit. Planet. Sci 51, 843–850.

Frank DR, Zolensky ME, and Le L (2014) Olivine in terminal particles of Stardust aerogel tracks and analogous grains in chondrite matrix. Geochim. Cosmochim. Acta 142, 240–259.

Friedrich JM, Weisberg MK, Ebel DS, Biltz AE, Corbett BM, Iotzov IV, Khan WS, and Wolman MD (2015) Chondrule size and related physical properties: A compilation and evaluation of current data across all meteorite groups. Chemie der Erde 75, 419–443.

Fu. RR and Elkins-Tanton LT (2014) The fate of magmas in planetesimals and the retention of primitive chondritic crusts. Earth Planet. Sci. Lett 390, 128–137.

Fuchs LH, Olsen E, and Jensen KJ (1973) Mineralogy, mineral-chemistry, and composition of the Murchison (C2) meteorite. Smithsonian Contributions to the Earth Sciences 10, 1–39.

Fujiya W, Sugiura N, Hotta H, Ichimura K, and Sano Y (2012) Evidence for the late formation of hydrous asteroids from young meteoritic carbonates. Nature Communications 3, 627.

Gerard O and Jaoul O (1989) Oxygen diffusion in San-Carlos olivine. J. Geophys. R. (Solid Earth) 94, 4119–4128.

Greenwood RC and Franchi IA (2004) Alteration and metamorphism of CO3 chondrites: Evidence from oxygen and carbon isotopes. Meteorit. Planet. Sci 39, 1823–1838.

Greenwood RC, Howard KT, Franchi IA, Zolensky ME, Buchanan PC, and Gibson (2014) Oxygen isotope evidence for the relationship between CM and CO chondrites: Could they both coexist on a single asteroid? In 45th Lunar and Planet. Sci. Conf. CD-ROM, p. #2610, abstr.

Gounelle M, Zolensky ME, Liou J-C, Bland PA, and Alard O (2003) Mineralogy of carbonaceous chondritic microclasts in howardites: Identification of C2 fossil micrometeorites. Geochim. Cosmochim. Acta 67, 507–527.

Grossman JN and Brearley AJ (2005) The onset of metamorphism in ordinary and carbonaceous chondrites. Meteorit. Planet. Sci 40, 87–122.

Grossman JW and Zipfel J (2001) The Meteoritical Bulletin, No 85. Meteorit. Planet. Sci 36, A293–A322.

Haack H, Grau T, Bischoff A, Horstmann M, Wasson J, Sørensen AN, Laubenstein M, Ott U, Palme H, Gellissen M, Greenwood RC, Pearson VK, Franchi IA, Gabelica Z, and Schmitt-Kopplin P (2012) Maribo - A new CM fall from Denmark. Meteorit. Planet. Sci 47, 30–50.

Hanowski NP and Brearley AJ (2001) Aqueous alteration of chondrules in the CM carbonaceous chondrite, Allan Hills 81002: Implications for parent body alteration. Geochim. Cosmochim. Acta 65, 495–518.

Heck PR, Ushikubo T, Schmitz B, Kita NT, Spicuzza MJ and Valley JW (2010) A single asteroidal source for extraterrestrial Ordivician chromite grains from Sweden and China: high-precision oxygen three-isotope SIMS analysis. Geochim. Cosmochim. Acta 74, 497–509.

Hertwig A, Defouilloy C, Kimura M, and Kita NT (2017) Oxygen isotope systematics of chondrule minerals from the reduced CV3 chondrite NWA 8613. In 48th Lunar and Planet. Sci. Conf. CD-ROM, p. #1227, abstr.

Hertwig A, Defouilloy C., and Kita NT (2018) Formation of chondrules in a moderately high dust enriched disk: Evidence from oxygen isotopes of chondrules from the Kaba CV3 chondrite. Geochim. Cosmochim. Acta 224, 116–131.

Hewins RH and Radomsky P (1990) Temperature conditions for chondrule formation. Meteoritics 25, 309–318.

Hewins RH and Zanda B (2012) Chondrules: Precursors and interactions with the nebular gas. Meteorit. Planet. Sci 47, 1120–1138.

Hewins RH, Bourot-Denise M, Zanda B, Leroux H, Barrat J-A, Humayun M, Göpel C, Greenwood RC, Franchi IA, Pont S, Lorand J-P, Cournède C, Gattacceca J, Rochette P, Kuga M, Marrocchi Y, and Marty B (2014) The Paris meteorite, the least altered CM chondrite so far. Geochim. Cosmochim. Acta 124, 190–222.

Jabeen I and Hiyagon H (2003) Oxygen isotopes in isolated and chondrule olivines of Murchison. In 34th Lunar and Planet. Sci. Conf., p. #1551, abstr.

Jenniskens P, Fries MD, Yin Q-Z, Zolensky M, Krot AN, Sandford SA, Sears D, Beauford R, Ebel DS, Friedrich JM, Nagashima K, Wimpenny J, Yamakawa A, Nishiizumi K, Hamajima Y, Caffee MW, Welten KC, Laubenstein M, Davis AM, Simon SB, Heck PR, Young ED, Kohl IE, Thiemens MH, Nunn MH, Mikouchi T, Hagiya K, Ohsumi K, Cahill TA, Lawton JA, Barnes D, Steele A, Rochette P, Verosub KL, Gattacceca J, Cooper G, Glavin DP, Burton AS, Dworkin JP, Elsila JE, Pizzarello S, Ogliore R, Schmitt-Kopplin P, Harir M, Hertkorn N, Verchovsky A, Grady M, Nagao K, Okazaki R, Takechi H, Hiroi T, Smith K, Silber EA, Brown PG, Albers J, Klotz D, Hankey M, Matson R, Fries JA, Walker RJ, Puchtel I, Lee C-T, Erdman ME, Eppich GR, Roeske S, Gabelica Z, Lerche M, Nuevo M, Girten B and Worden SP (2012) Radar enabled recovery of the Sutter's Mill meteorite, a carbonaceous chondrite regolith breccia. Science 338, 1583–1587. [PubMed: 23258889]

Jones RH (1992) On the relationship between isolated and chondrule olivine grains in the carbonaceous chondrite ALHA77307. Geochim. Cosmochim. Acta 56, 467–482.

Jones RH (1994) Petrology of FeO-poor, porphyritic pyroxene chondrules in the Semarkona chondrite. Geochim. Cosmochim. Acta 60, 3115–3138.

Jones RH, Leshin LA, Guan Y, Sharp ZD Durakiewicz T, and Schilk (2004) Oxygen isotope heterogeneity in chondrules from the Mokoia CV3 carbonaceous chondrite. Geochim. Cosmochim. Acta 68, 3423–3438.

Jones RH (2012) Petrographic constraints on the diversity of chondrule reservoirs in the protoplanetary disk. Meteorit. Planet. Sci 47, 1176–1190.

Kallemeyn GW and Wasson JT (1981) The compositional classification of chondrites: I. The carbonaceous chondrite groups. Geochim. Cosmochim. Acta 45, 1217–1230.

Keller LP and Buseck PR (1990) Matrix mineralogy of the Lancé CO3 carbonaceous chondrite: A transmission electron microscope study. Geochim. Cosmochim. Acta 54, 1155–1163.

Kimura M, Grossman JN, and Weisberg MK (2008) Fe-Ni metal in primitive chondrites: Indicators of classification and metamorphic conditions for ordinary and CO chondrites. Meteorit. Planet. Sci 43, 1161–1177.

Kita NT and Ushikubo T (2012) Evolution of protoplanetary disk inferred from 26Al chronology of individual chondrules. Meteorit. Planet. Sci 47, 1108–1119.

Kita NK, Kimura M, Ushikubo T, Valley JW, and Nyquist LE (2008) Oxygen isotope systematics of chondrules from the least equilibrated H chondrite. In 39th Lunar and Planet. Sci. Conf. CD-ROM, p. #2059, abstr.

Kita NT, Ushikubo T, Fu B and Valley JW (2009) High precision SIMS oxygen isotope analysis and the effect of sample topography. Chem. Geol 264, 43–57.

Kita NT, Nagahara H, Tachibana S, Tomomura S, Spicuzza MJ, Fournelle JH and Valley JW (2010) High precision SIMS oxygen three isotope study of chondrules in LL3 chondrites: role of ambient gas during chondrule formation. Geochim. Cosmochim. Acta 74, 6610–6635.

Kita NT, Tenner TJ, Defouilloy C, Nakashima D, Ushikubo T, and Bischoff A (2015) Oxygen isotope systematics of chondrules in R3 clasts: A genetic link to ordinary chondrites. In 46th Lunar and Planet. Sci. Conf. CD-ROM, p. #2053, abstr.

Kita NT, Tenner TJ, Ushikubo T, Hertwig A, Chaumard N, Defouilloy C, Nakashima D, Rudraswami NG, Weisberg MK, Kimura M, Nagahara H, and Bischoff A (2016) Chondrule oxygen isotope systematics among different chondrite groups: variety of isotope reservoirs in the protoplanetary disk. In 79th Annual Meteoritical Society Meeting, p. #6378, abstr.

Krot AN, Hutcheon ID, Yurimoto H, Cuzzi JN, McKeegan KD, Scott ERD, Libourel G, Chaussidon M, Aléon J, and Petaev MI (2005) Evolution of oxygen isotopic composition in the inner solar nebula. Astrophys. J 622, 1333–1342.

Krot AN, Yurimoto H, McKeegan KD, Leshin L, Chaussidon M, Libourel G, Yoshitake M, Huss GR, Guan Y, and Zanda B (2006a) Oxygen isotopic compositions of chondrules: implications for evolution of oxygen isotopic reservoirs in the inner Solar nebula. Chem. Erde 66, 249–176.

Krot AN, Hutcheon ID, Brearley AJ, Pravdivtseva OV, Petaev MI, and Hohenberg CM (2006b) Timescales and setting for alteration of chondritic meteorites In Meteorites and the Early Solar System II, edited by Lauretta DS and McSween HY, Jr. Tucson, Arizona: University of Arizona Press pp. 525–553.

Krot AN, Nagashima K, Yoshitake M, and Yurimoto H (2010) Oxygen isotopic compositions of chondrules from the metal-rich chondrites Isheyevo (CH/CBb), MAC 02675 (CBb), and QUE 94627 (CBb). Geochim. Cosmochim. Acta 74, 2190–2211.

Krot AN and Nagashima K (2017) Constraints on mechanisms of chondrule formation from chondrule precursors and chronology of transient heating events in the protoplanetary disk. Geochem. J 51, 45–68.

Kunihiro T, Rubin AE, McKeegan KD and Wasson JT (2004a) Oxygen-isotopic compositions of relict and host grains in chondrules in the Yamato 81020 CO3.0 chondrite. Geochim. Cosmochim. Acta 68, 3599–3606.

Kunihiro T, Rubin AE, McKeegan KD, and Wasson JT (2004b) Initial 26Al/27Al in carbonaceous chondrite chondrules: Too little 26Al to melt asteroids. Geochim. Cosmochim. Acta 68, 2947–2957.

Kunihiro T, Rubin AE and Wasson JT (2005) Oxygen-isotopic compositions of low-FeO relicts in high FeO-host chondrules in Acfer 094, a type 3.0 carbonaceous chondrite closely related to CM. Geochim. Cosmochim. Acta 69, 3831–3840.

Kurahashi E, Kita NT, Nagahara H, and Morishita Y (2008) ^{26}Al-^{26}Mg systematics of chondrules in a primitive CO chondrite. Geochim. Cosmochim. Acta 72, 3865–3882.

Lee MR and Lindgren P (2016) Aqueous alteration of chondrules from the Murchison CM carbonaceous chondrite: Replacement, pore filling, and the genesis of polyhedral serpentine. Meteorit. Planet. Sci 51, 1003–1021.

Libourel G, Krot AN, and Tissandier L (2006) Role of gas-melt interaction during chondrule formation. Earth Planet. Sci. Lett 251, 232–240

Libourel G and Chaussidon M (2011) Oxygen isotopic constraints on the origin of Mg-rich olivines from chondritic meteorites. Earth Planet. Sci. Lett 301, 9–21.

Lindgren P, Lee MR, Starkey NA, and Franchi IA (2017) Fluid evolution in CM carbonaceous chondrites tracked through the oxygen isotopic compositions of carbonates. Geochim. Cosmochim. Acta 204, 240–251.

Lofgren GE (1996) A dynamic crystallization model for chondrule melts In Chondrules and the Protoplanetary Disk, edited by Hewins RH, Jones RH, and Scott ERD Cambridge, UK: Cambridge University Press, pp. 187–196.

Lunine JI (2006) Origin of water ice in the Solar System In Meteorites and the Early Solar System II, edited by Lauretta DS and McSween HY, Jr. Tucson, Arizona: University of Arizona Press pp. 309–319.

Mackinnon IDR and Zolensky ME (1984) Proposed structures for poorly characterized phases in C2M carbonaceous chondrite meteorites. Nature 309, 240–242.

MacPherson GJ, Kita NT, Ushikubo T, Bullock ES, and Davis AM (2012) Well-resolved variations in the formation ages for Ca-Al-rich inclusions in the early solar system. Earth Planet. Sci. Lett 331-332, 43–54.

Marrocchi Y and Chaussidon M (2015) A systematic for oxygen isotopic variation in meteoritic chondrules. Earth Planet. Sci. Lett 430, 308–315.

Martin RG and Livio M (2012) On the evolution of the snow line in protoplanetary disks. Monthly Notices Letters of the Royal Astromomical Society 425, L6–L9.

May C, Russell SS, and Grady MM (1999) Analysis of chondrule and CAI size and abundance in CO3 and CV3 chondrites: a preliminary study. In 30th Lunar and Planet. Sci. Conf., p. #1688, abstr.

McSween HY (1979) Alteration in CM carbonaceous chondrites inferred from modal and chemical variations in matrix. Geochim. Cosmochim. Acta 43, 1761–1770.

Min M, Dullemond CP, Kama M, and Dominik C (2011) The thermal structure and the location of the snow line in the protosolar nebula: Axisymetric models with full 3-D radiative transfer. Icarus 212, 416–426.

Morbidelli A, Gounelle M, Levison HF, and Bottke WF (2006) Formation of the binary near-Earth object 1996 FG_3: Can binary NEOs be the source of short-CRE meteorites? Meteorit. Planet. Sci 41, 875–887.

Morris MA and Desch SJ 2010 Thermal histories of chondrules in solar nebula shocks. Astrophys. J 722, 1474–1494.

Nakashima D, Kimura M, Yamada K, Noguchi T, Ushikubo T, and Kita NT (2010) Study of chondrules in CH chondrites - I: Oxygen isotope ratios of chondrules. In 73rd Annual Meteoritical Society Meeting, p. #5288, abstr.

Nakashima D, Ushikubo T, Gowda RN, Kita NT, Valley J, and Nagao K (2011) Ion microprobe analyses of oxygen three-isotope ratios of chondrules from the Sayh al Uhaymir 290 CH chondrite using a multiple-hole disk. Meteorit. Planet. Sci 46, 857–874.

Nagahara H, Kita NT, Ozawa K, and Morishita Y (2008) Condensation of major elements during chondrule formation and its implication to the origin of chondrules. Geochim. Cosmochim. Acta 72, 1442–1465.

Nagashima K, Krot AN, and Huss GR (2015) Oxygen-isotope compositions of chondrule phenocrysts and matrix grains in Kakangari K-grouplet chondrite: Implication to a chondrule-matrix genetic relationship. Geochim. Cosmochim. Acta 151, 49–67.

Oka A, Nakamoto T, and Ida S (2011) Evolution of snow line in optically thick protoplanetary disks: Effects of water ice opacity and dust grain size. Astrophys. J 738, 141.

Ozawa K and Nagahara H (2001) Chemical and isotopic fractionations by evaporation and their cosmochemical implications. Geochim. Cosmochim. Acta 65, 2171–2199.

Radomsky PM and Hewins RH (1990) Formation conditions of pyroxene-olivine and magnesian olivine chondrules. Geochimica et Cosmochimica Acta 54, 3475–3490.

Rubin AE (1989) Size-frequency distributions of chondrules in CO3 chondrites. Meteoritics 24, 179–189.

Rubin AE (1998) Correlated petrologic and geochemical characteristics of CO3 chondrites. Meteor. Planet. Sci 33, 385–391.

Rubin AE (2010) Physical properties of chondrules in different chondrites groups: Implications for multiple melting events in dusty environment. Geochim. Cosmochim. Acta 74, 4807–4828.

Rubin AE and Wasson JT (1986) Chondrules in the Murray CM2 meteorite and compositional differences between CM-CO and ordinary chondrite chondrules. Geochim. Cosmochim. Acta 50, 307–315.

Rubin AE, Trigo-Rodríguez JM, Huber H, and Wasson JT (2007) Progressive aqueous alteration of CM carbonaceous chondrites. Geochim. Cosmochim. Acta 71, 2361–2382.

Rudraswami NG, Ushikubo T, Nakashima D and Kita NT (2011) Oxygen isotope systematics of chondrules in the Allende CV3 chondrite: high precision ion microprobe studies. Geochim. Cosmochim. Acta 75, 7596–7611.

Russell SS, Krot AN, MacPherson GJ, Huss GR, Itoh S, Yurimoto H, and Keil K (2005) Genetic relation-ship between refractory inclusions and chondrules In Chondrites and the Protoplanetary Disk, edited by Krot AN, Scott ERD, and Reipurth B. ASP Conference Series 341, 317–353.

Ruzicka A, Hiyagon H, Hutson M, and Floss C (2007) Relict olivine, chondrule recycling, and the evolution of nebular oxygen reservoirs. Earth Planet. Sci. Lett 257, 274–289.

Ruzicka A, Floss C, and Hutson M (2008) Relict olivine grains, chondrules recycling, and implications for the chemical, thermal, and mechanical processing of nebular materials. Geochim. Cosmochim. Acta 72, 5530–5557.

Ryerson FJ, Durham WB, Cherniak DJ, Lanford WA (1989) Oxygen diffusion in olivine - Effect of oxygen fugacity and implications fro creep. J. Geophys. R. (Solid Earth) 94, 4105–4118.

Sanborn ME, Yin Q-Z, Irving AJ, and Bunch TE (2015) Differentiated planetesimals with chondritic crusts: Δ17O-ε54Cr evidence in unique, ungrouped achondrites for partial melting of the CV/CK and CO parent bodies. In 46th Lunar and Planet. Sci. Conf. CD-ROM, p. #2259, abstr.

Schrader DL and Davidson J (2017) CM and CO chondrites: A common parent body or asteroidal neighbors? Insights from chondrule silicates. Geochim. Cosmochim. Acta 214, 157–171.

Schrader DL, Connolly HC, Jr., and Lauretta DS (2008) Opaque phases in type-II chondrules from CR2 chondrites: Implications for CR parent body formation. Geochim. Cosmochim. Acta 72, 6124–6140.

Schrader DL, Connolly HC, Jr., Lauretta DS, Nagashima K, Huss GR, Davidson J and Domanik KJ (2013) The formation and alteration of the Renazzo-like carbonaceous chondrites II: linking O-isotope composition and oxidation state of chondrule olivine. Geochim. Cosmochim. Acta 101, 302– 327.

Schrader DL, Nagashima K, Krot AN, Ogliore RC, and Hellebrand E (2014) Variations in the O-isotope composition of gas during the formation of chondrules from the CR chondrites. Geochim. Cosmochim. Acta 132, 50–74.

Schrader DL, Connolly HC, Jr., Lauretta DS, Zega TJ, Davidson J, Domanik KJ (2015) The formation and alteration of the Renazzo-like carbonaceous chondrites III: Toward understanding the genesis of ferromagnesian chondrules. Meteorit. Planet. Sci 50, 15–50.

Schrader DL, Nagashima K, Krot AN, Ogliore RC, Yin Q-Z, Amelin Y, Stirling CH, Kaltenbach A (2017a) Distribution of ^{26}Al in the CR chondrite chondrule-forming region of the protoplanetary disk. Geochim. Cosmochim. Acta 201, 275–302.

Schrader DL, Fu RR, Davidson J, and Ogliore RC (2017b) Evidence for chondrule migration from dusty olivine chondrules. In 48th Lunar and Planet. Sci. Conf. CD-ROM, p. #1271, abstr.

Scott ERD and Taylor JG (1983) Chondrules and other components in C, O, and E chondrites: Similarities in their properties and origins. In *Proceedings,* 14th Lunar and Planetary Science Conference, J. Geophys. Res 88, B275–B286.

Scott ERD, Love SG, and Krot AN (1996) Formation of chondrules and chondrites in the protoplanetary nebula In Chondrules and the Protoplanetary Disk, edited by Hewins RH, Jones RH, and Scott ERD Cambridge, UK: Cambridge University Press pp. 87–96.

Sears DWG and Dodd RT (1988) Overview and classification of meteorites In Meteorites and the early solar system, edited by Kerridge JF and Matthews MS Tucson: University of Arizona Press pp 3–31.

Shibata Y and Matsueda H (1994) Chemical composition of Fe-Ni metal and phosphate minerals in Yamato-82094 carbonaceous chondrite. Proc. NIPR Symp. Antarct. Meteorit 7, 110–124.

Sugiura N and Fujiya W (2014) Correlated accretion ages and ε^{54}Cr of meteorite parent bodies and the evolution of the solar nebula. Meteorit. Planet. Sci 49, 772–787.

Tachibana S, Nagahara H, Mostefaoui S, and Kita NT (2003) Correlation between relative ages inferred from ^{26}Al and bulk compositions of ferromagnesian chondrules in least equilibrated ordinary chondrites. Meteorit. Planet. Sci 38, 939–962.

Tenner TJ, Nakashima D, Ushikubo T, Kita NT, and Weisberg WK (2012) Oxygen isotopes of chondrules in the Queen Alexandra Range 99177 CR3 chondrite: Further evidence for systematic relationships between chondrule Mg# and Δ17O and the role of ice during chondrule formation. In 43rd Lunar and Planet. Sci. Conf. CD-ROM, p. #2127, abstr.

Tenner TJ, Ushikubo T, Kurahashi E, Kita NT and Nagahara H (2013) Oxygen isotope systematics of chondrule phenocrysts from the CO3.0 chondrite Yamato 81020: evidence for two distinct oxygen isotope reservoirs. Geochim. Cosmochim. Acta 102, 226–245.

Tenner TJ, Nakashima D, Ushikubo T, Kita NT and Weisberg MK (2015) Oxygen isotope ratios of Fe-poor chondrules in CR3 chondrites: Influence of dust enrichment and H_2O during chondrule formation. Geochim. Cosmochim. Acta 148, 228–250.

Tenner TJ, Kimura M, and Kita NT (2017) Oxygen isotope characteristics of chondrules from the Yamato-82094 ungrouped carbonaceous chondrite: Further evidence for common O-isotope environments sampled among carbonaceous chondrites. Meteorit. Planet. Sci, 52, 268–294.

Tissandier L, Libourel G, and Robert F (2002) Gas-melt interactions and their bearing on chondrule formation. Meteorit. Planet. Sci 37, 1377–1389.

Tomeoka K and Buseck PR (1985) Indicators of aqueous alteration in CM carbonaceous chondrites: microtextures of a layered mineral containing Fe, S, O, and Ni. Geochim. Cosmochim. Acta 49, 2149–2163.

Ushikubo T, Kimura M, Kita NT and Valley JW (2012) Primordial oxygen isotope reservoirs of the solar nebula recorded in chondrules in Acfer 094 carbonaceous chondrite. Geochim. Cosmochim. Acta 90, 242–264.

Ushikubo T, Nakashima D, Kimura M, Tenner TJ, and Kita NT (2013) Contemporaneous formation of chondrules in distinct oxygen isotope reservoirs. Geochim. Cosmochim. Acta 109, 280–295.

Van Orman JA, Cherniak DJ, and Kita NT (2014) Magnesium diffusion in plagioclase: Dependence on composition, and implications for thermal resetting of the ^{26}Al-^{26}Mg early solar system chronometer. Earth Planet. Sci. Lett 385, 79–88.

Verdier-Paoletti MJ, Marrocchi Y, Avice G, Roskosz M, Gurenko A, and Gounelle M (2017) Oxygen isotope constraints on the alteration temperatures of CM chondrites. Earth Planet. Sci. Lett 458, 273–281.

Villeneuve J, Libourel G, and Soulié C (2015) Relationships between type I and type II chondrules: Implications on chondrule formation processes. Geochim. Cosmochim. Acta 160, 277–305.

Wasson JT and Rubin AE (2003) Ubiquitous low-FeO relict grains in type II chondrules and limited overgrowths on phenocrysts following the final melting event. Geochim. Cosmochim. Acta 67, 2239–2250.

Wasson JT, Rubin AE and Yurimoto H (2004) Evidence in CO3.0 chondrules for a drift in the O isotopic composition of the solar nebula. Meteorit. Planet. Sci 39, 1591–1598.

Weisberg MK, Prinz M, Clayton RN, and Mayeda TK (1993) The CR (Renazzo-type) carbonaceous chondrite group and its implications. Geochim. Cosmochim. Acta 57, 1567–1586.

Weisberg MK, McCoy TJ, and Krot AN (2006) Systematics and evaluation of meteorite classification In Meteorites and the Early Solar System II, edited by Lauretta DS and McSween HY, Jr. Tucson, Arizona: University of Arizona Press pp. 19–52.

Weisberg MK, Ebel DS, Kimura M, Kita NT, and Nakashima D (2010) Petrology and oxygen isotopes of chondrules in the Kota EH3 chondrite. In 41st Lunar and Planet. Sci. Conf. CD-ROM, p. #1756, abstr.

Weisberg MK, Ebel DS, Connolly HC, Jr., Kita NT, and Ushikubo T (2011) Petrology and oxygen isotope compositions of chondrules in E3 chondrites. Geochim. Cosmochim. Acta 75, 6556–6569.

Young ED and Russell SS (1998) Oxygen reservoirs in the early solar nebula inferred from an Allende CAI. Science 282, 1874–1877.

Yu Y, Hewins RH, Clayton RN, and Mayeda TK (1995) Experimental study of high temperature oxygen isotope exchange during chondrule formation. Geochim. Cosmochim. Acta 59, 2095–2104.

Zanda B, Bourot-Denise M, Perron C, and Hewins RH (1994) Origin and metamorphic redictribution of silicon, chromium, and phosphorous in the metal of chondrites. Science 256, 1846–1849.

Zanda B, Bourot-Denise M, Hewins RH, Cohen BA, Delaney JS, Humayun M, and Campbell AJ (2002) Accretion textures, iron evaporation and re-condensation in Renazzo chondrules. In 33rd Lunar and Planet. Sci. Conf. *CD-ROM*, p. #1852, abstr.

Zanda B, Hewins RH, Bourot-Denise M, Bland PA, and Albarède F (2006) Formation of solar nebula reservoirs by mixing chondritic components. Earth Planet. Sci. Lett 248, 650–660.

Zhang A-C, Itoh S, Sakamoto N, Wang R-C, and Yurimoto H (2014) Origins of Al-rich chondrules: Clues from a compound Al-rich chondrule in the Dar al Gani 978 carbonaceous chondrite. Geochim. Cosmochim. Acta 130, 78–92.

Zolensky M and McSween HY, Jr. (1988) Aqueous alteration. In Meteorites and the Early Solar System, edited by Kerridge JF and Matthews MS Tucson, Arizona: University of Arizona Press pp. 114–143.

Zolensky ME, Barrett R, and Browning L (1993) Mineralogy and composition of matrix and chondrule rims in carbonaceous chondrites. Geochim. Cosmochim. Acta 57, 3123–3148.

Zolensky ME, Weisberg MK, Buchanan PC, Mittlefehldt DW (1996) Mineralogy of carbonaceous chondrite clasts in HED achondrites and the Moon. Meteorit. Planet. Sci 31, 518–537.

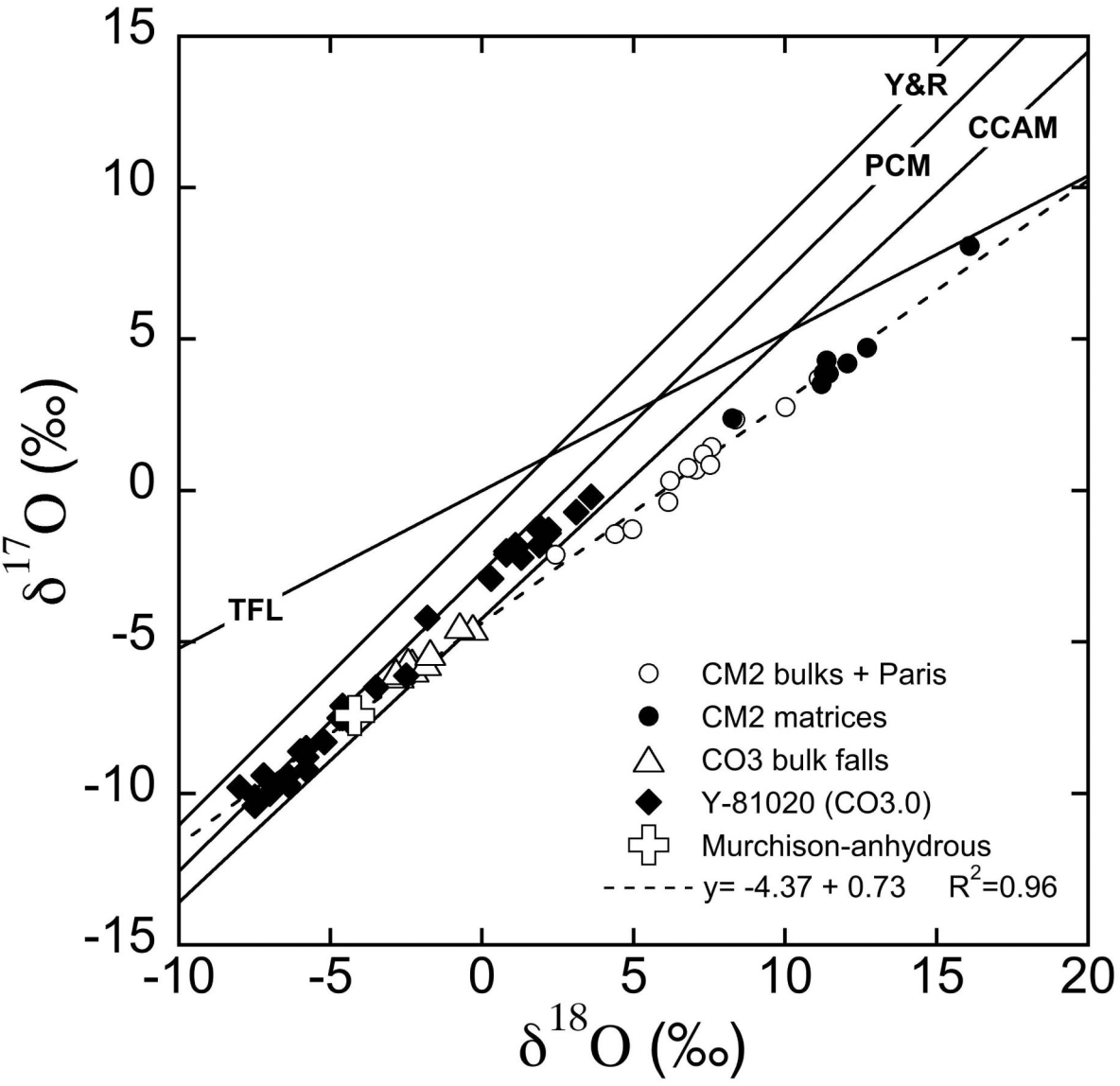

Fig. 1.

Oxygen three-isotope diagram of bulk and chondritic components from CM and CO chondrites. The CCAM (carbonaceous chondrite anhydrous mineral; Clayton et al., 1977), Y&R (Young and Russell, 1998), and PCM (primitive chondrule minerals; Ushikubo et al., 2012) lines are shown for reference. The terrestrial fractionation line (TFL) is also shown. CM2 bulk data include falls data from Clayton and Mayeda (1999) and the two falls Sayama (Grossman and Zipfel, 2001) and Maribo (Haack et al., 2012). Both altered and less altered lithologies from the CM2 Paris are reported (Hewins et al., 2014). CM2 matrices and CO3 bulk falls are from Clayton and Mayeda (1999) and Greenwood and Franchi (2004), respectively. The Murchison-anhydrous data are from anhydrous mineral separates of the Murchison CM2 chondrite (Clayton and Mayeda, 1984). Y-81020 data are SIMS olivine and pyroxene analyses from chondrules in the Yamato 81020 CO3.0 chondrite (Tenner et al., 2013). The dashed line indicates the linear regression through the oxygen isotope data for the CM2 bulk compositions, Paris, and the anhydrous mineral separates of Murchison.

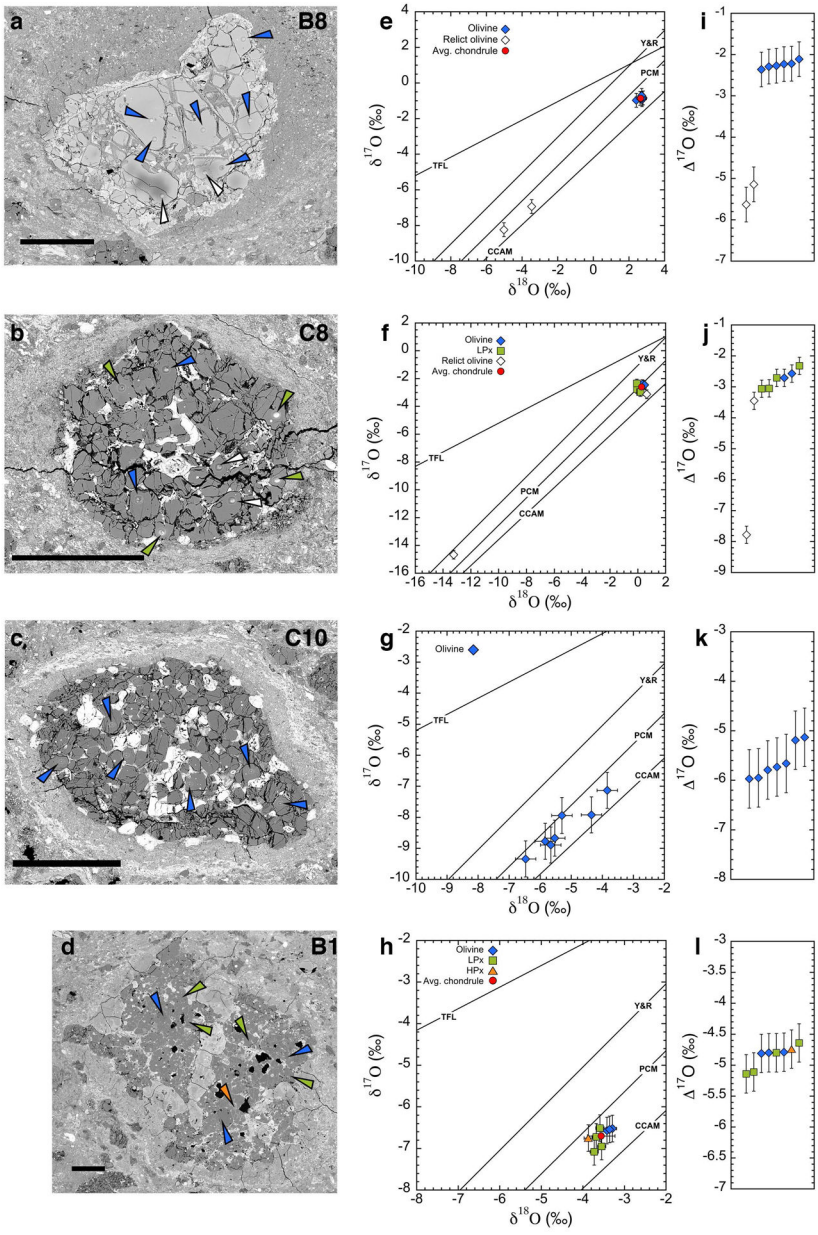

Fig. 2.

Examples of SIMS oxygen three-isotope analyses of chondrules in Murchison. a–d) Backscattered electron images of chondrules B8 (type II), C8 (type I, GOP), C10 (type I, GO), and B1 (type I, PP), respectively. Analysis points are shown by the vertex of the triangles, color-coded for mineral phases (olivine: blue, relict olivine: black, low-Ca pyroxene: green, and high-Ca pyroxene: orange). Scale bars are 150 μm. e-h) Oxygen three-isotope diagrams of individual spot analyses in chondrules B8, C8, C10, and B1, respectively. Except for the heterogeneous chondrule C10 (g), the average values of multiple analyses excluding relict olivine grains are shown as red circles. The four reference lines are the same as in Fig. 1. i-l) $\Delta^{17}O$ values of individual analyses from chondrules B8, C8, C10, and B1, respectively. Data are shown in ascending sequence. Symbols are the same as in

oxygen three-isotope plots. Error bars in the oxygen three-isotope and $\Delta^{17}O$ value plots are at 95% confidence level, which are shown in EA4.

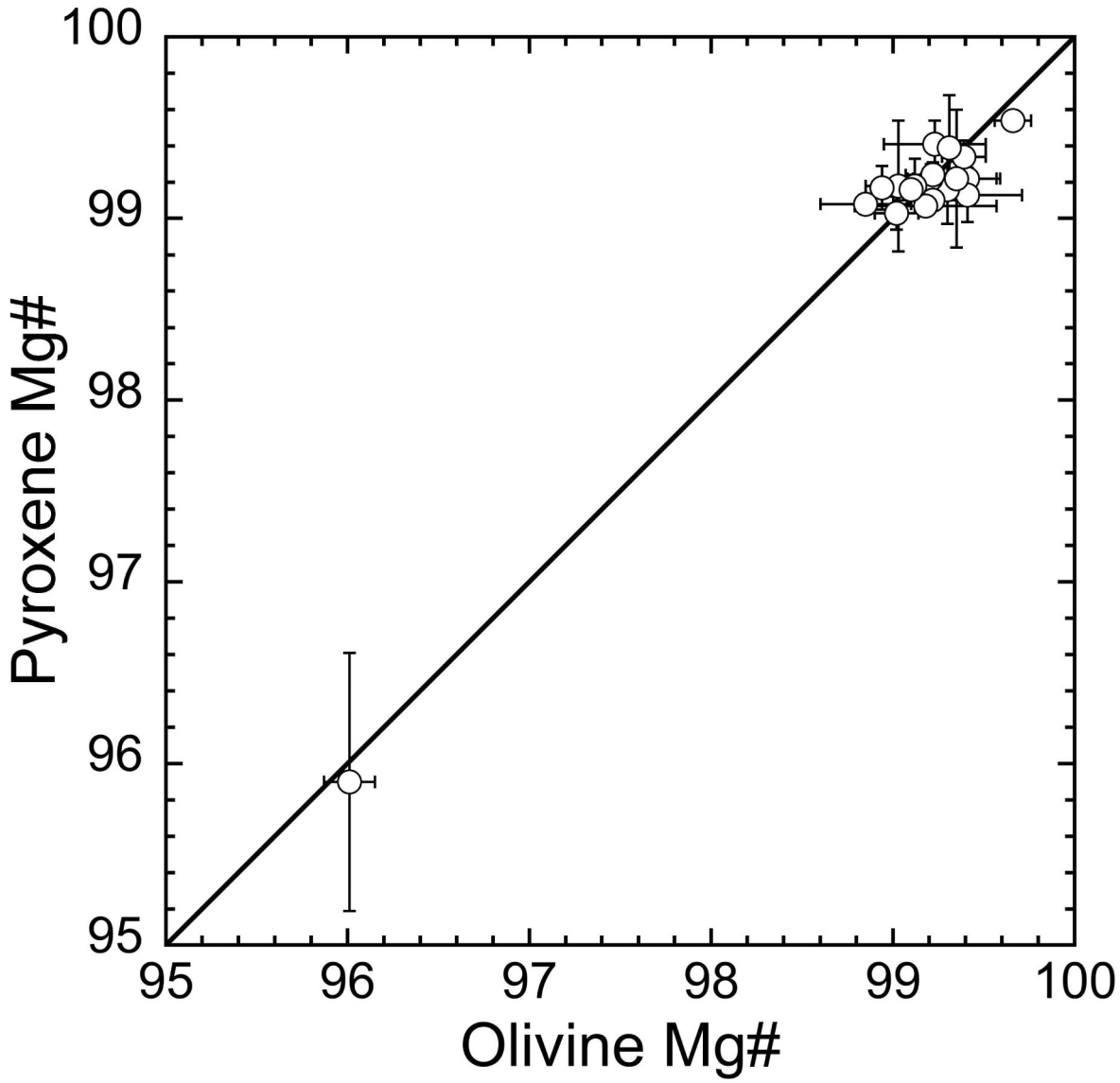

Fig. 3.

Comparison between olivine and low Ca-pyroxene Mg#'s in 19 type I chondrules from Murchison. Each point corresponds to the averaged Mg# of olivine and low-Ca pyroxene coexisting within a single chondrule. Error bars correspond to 2SD of multiple analyses. A 1:1 line is shown for reference.

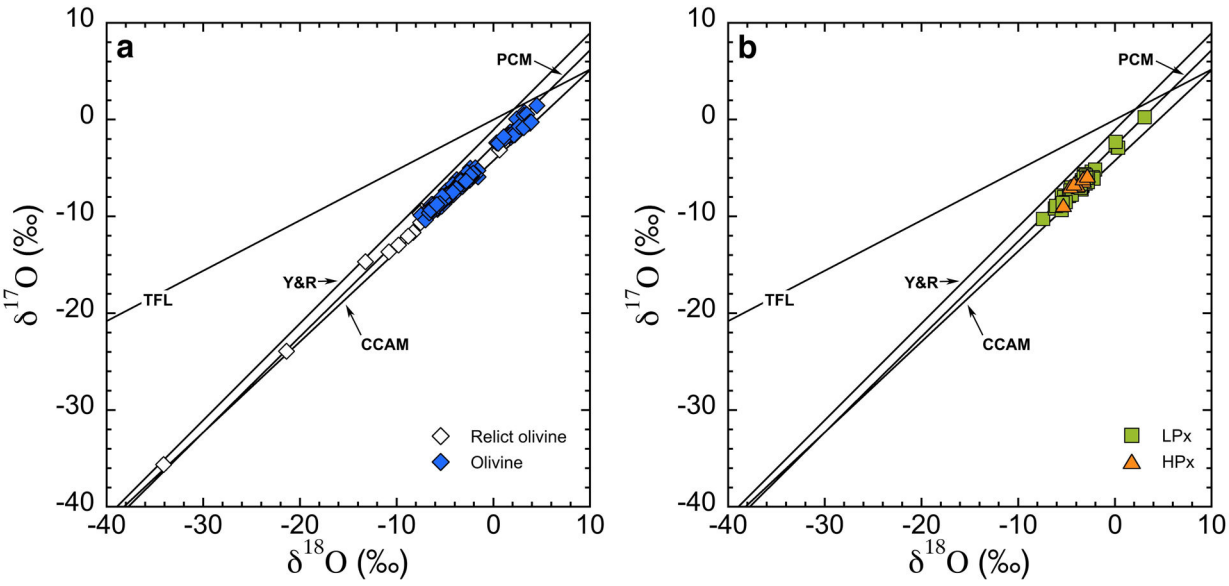

Fig. 4.

Oxygen three-isotope diagram of individual spot analyses of chondrules in Murchison. a) olivine. Relict olivine grains are shown as open symbols. b) pyroxene. Low-Ca pyroxene (LPx): squares, high-Ca pyroxene (HPx): triangles. Uncertainties of individual data, corresponding to the spot-to-spot reproducibility (2SD), are smaller than the size of symbols. The four reference lines are the same as in Fig. 1.

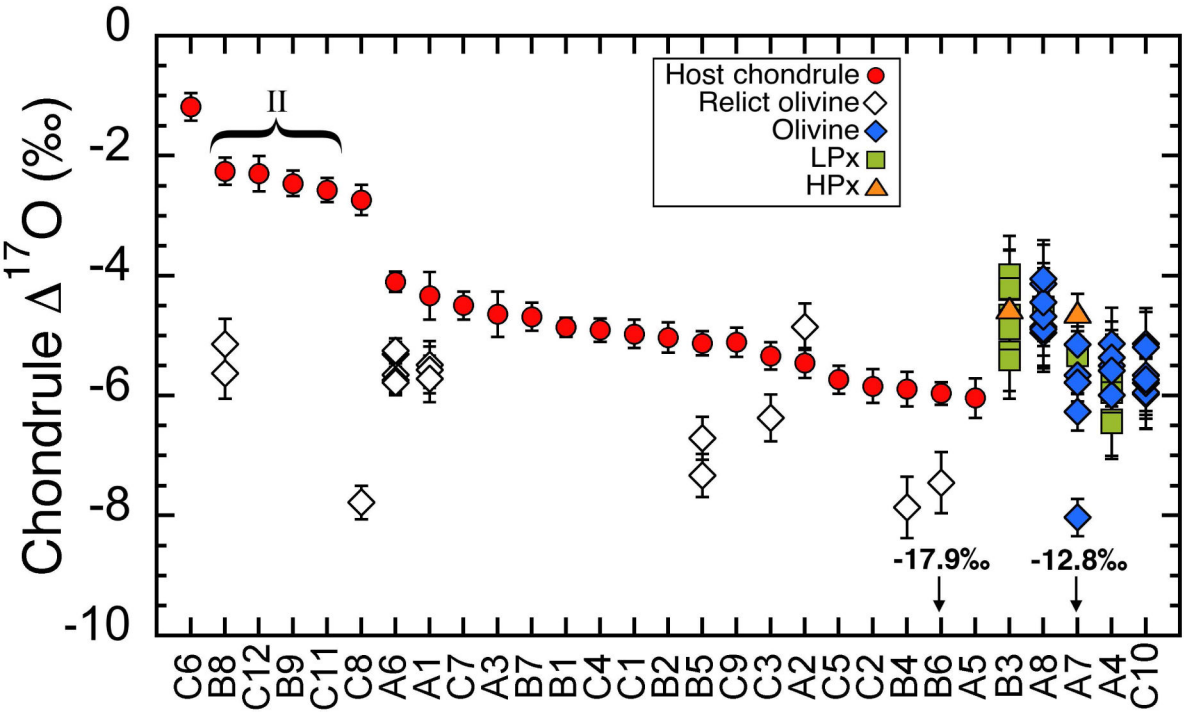

Fig. 5.

$\Delta^{17}O$ values of individual host chondrules in Murchison. Relict olivine grains are shown together. Data are from Tables 1 and 2. The homogeneous chondrule data are sorted following the host $\Delta^{17}O$ values. For heterogeneous chondrules (B3, A8, A7, A4, and C10), individual analyses within each chondrule are shown.

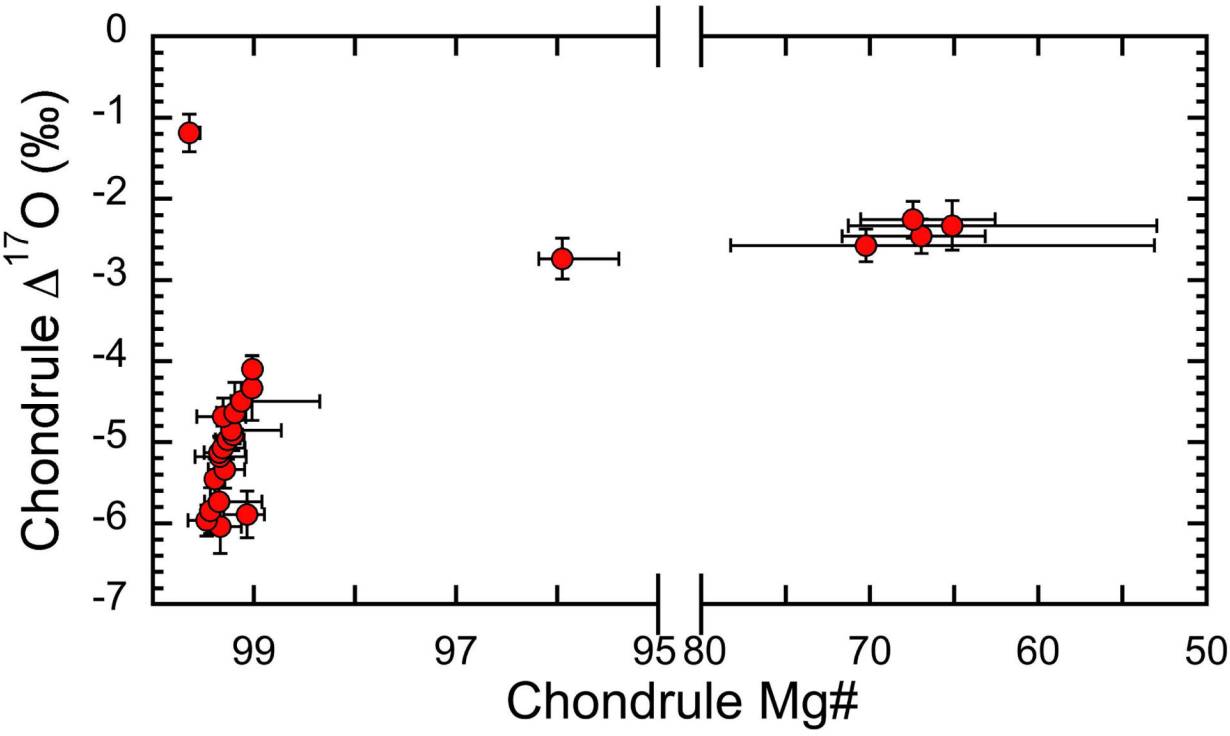

Fig. 6.

Murchison chondrule $\Delta^{17}O$ values vs. Mg#'s. Each point represents the host Mg# and $\Delta^{17}O$ values of individual chondrules. Chondrule Mg# uncertainties correspond to the range of measured values, while uncertainties in $\Delta^{17}O$ are those of the mean value at 95% confidence level, shown in EA4.

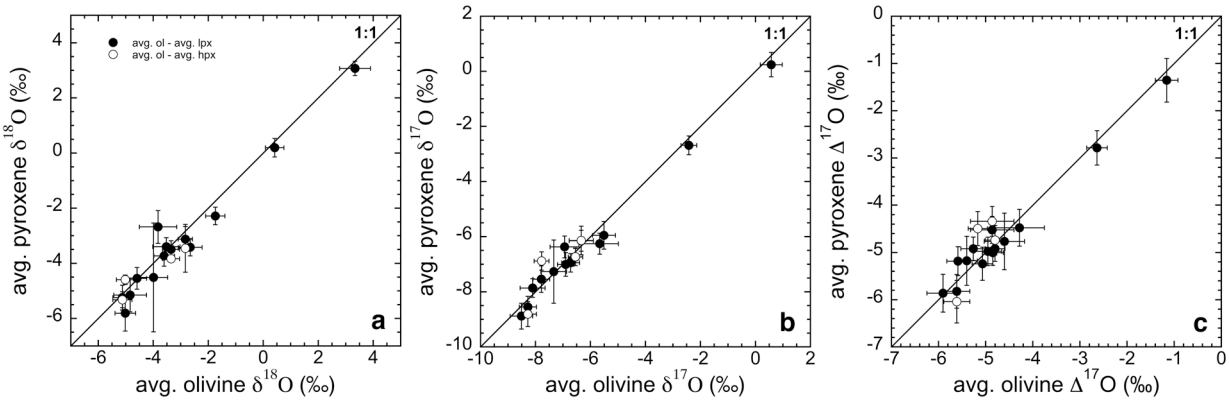

Fig. 7.

Comparison of oxygen isotope ratios between coexisting olivine and pyroxene from 15 individual chondrules in Murchison. The mean low-Ca and high-Ca pyroxene data are plot against the mean olivine data for $\delta^{18}O$ (a), $\delta^{17}O$ (b), and $\Delta^{17}O$ (c). Relict grains are not included in the calculation of mean values. Propagated uncertainties are estimated in the same procedure as host chondrule calculations (see EA4).

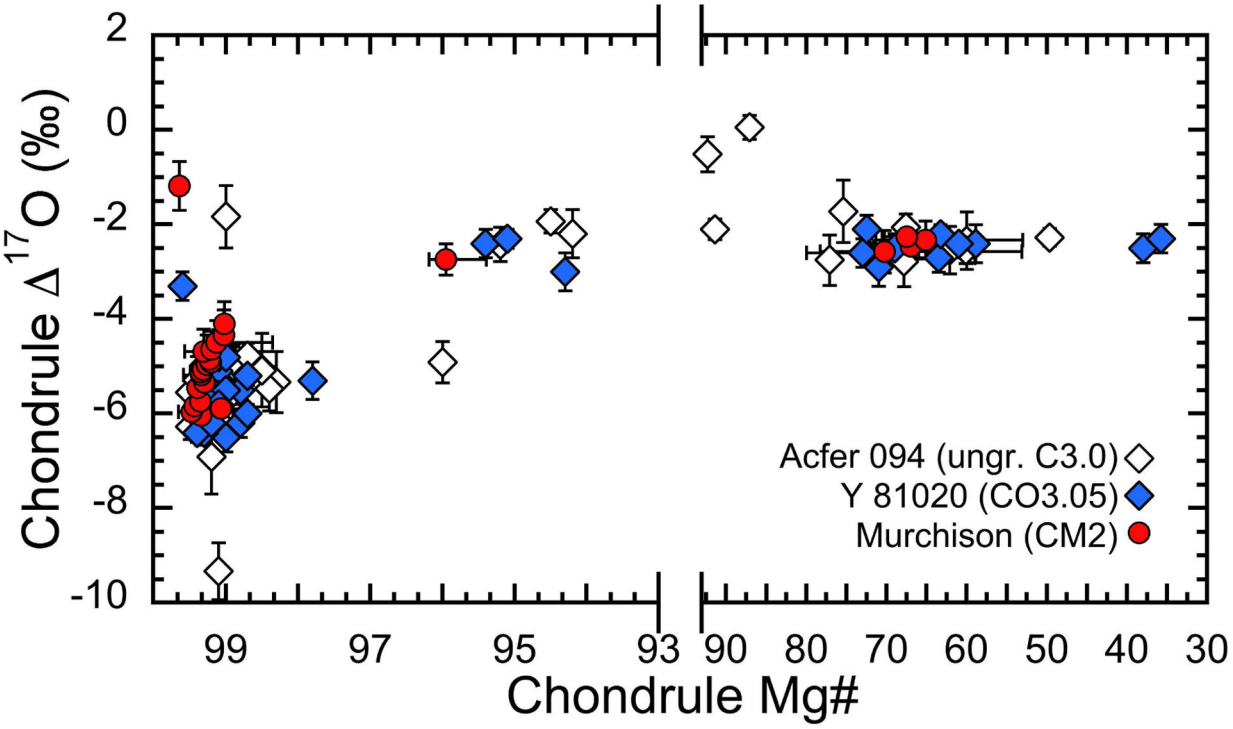

Fig. 8.

Comparison of the Mg# and $\Delta^{17}O$ relationships of chondrules from Murchison (this work), Acfer 094 (ungrouped C3.00; Ushikubo et al., 2012), and the Y-81020 (CO3.05; Tenner et al., 2013).

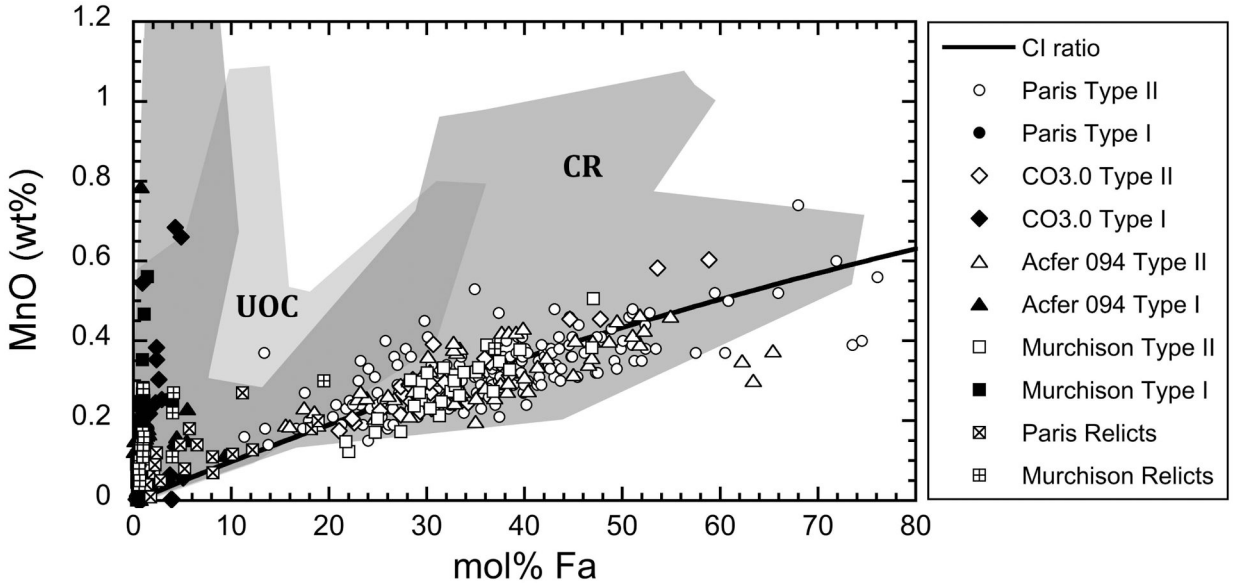

Fig. 9.

MnO (wt%) vs. mol.% Fa for olivine grains in chondrules from Murchison. Data from CO3.0 (Jones, 1992), Acfer 094 (Ushikubo et al., 2012), and Paris (Hewins et al., 2014) are shown for comparison, as well as the fields defined by the CR (Berlin et al., 2011; Frank et al., 2014; Schrader et al., 2015) and unequilibrated ordinary chondrites (UOC) (Frank et al., 2014; and references therein). The CI ratio is represented by the solid line (data from Anders and Grevesse, 1989).

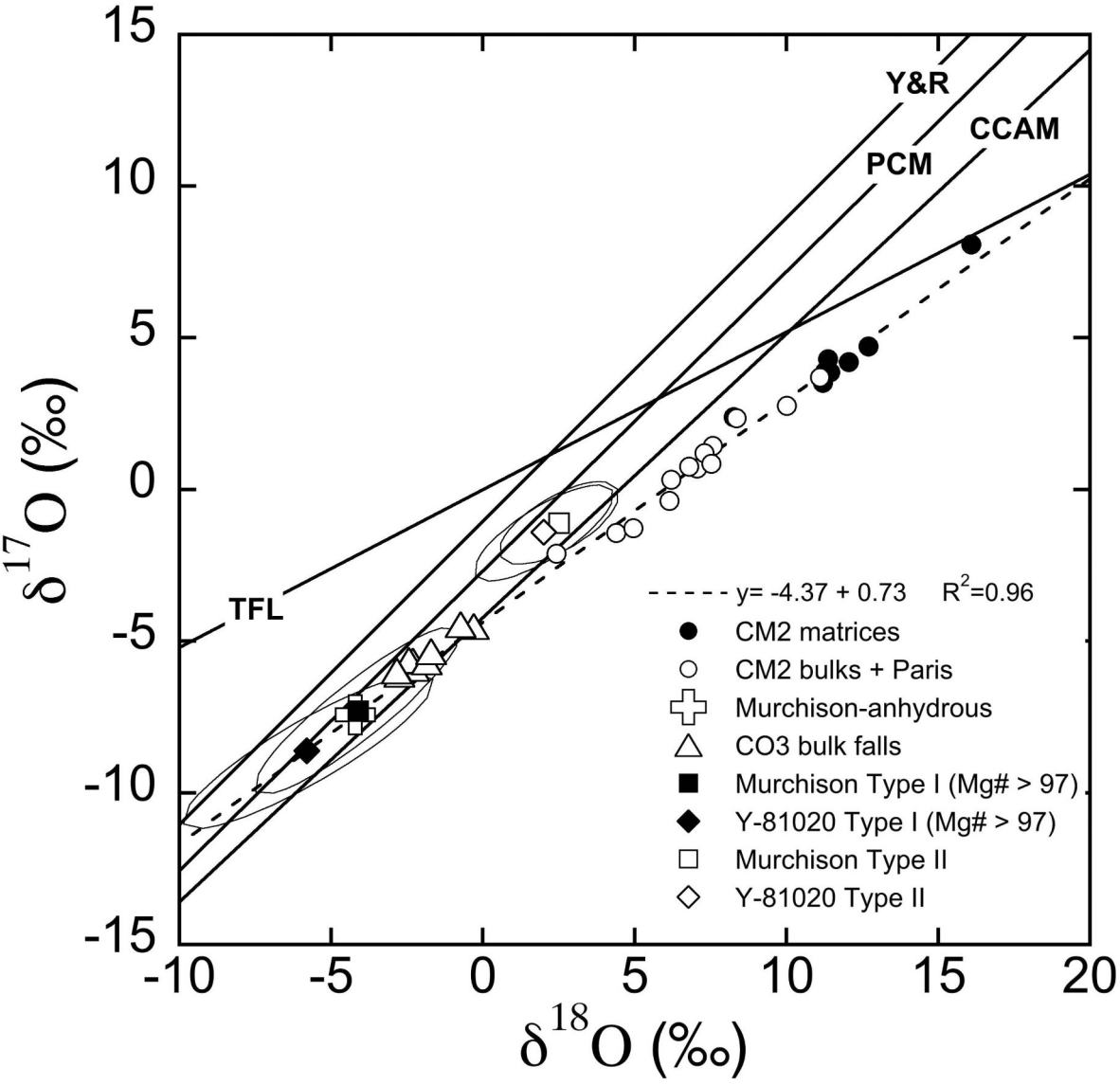

Fig. 10.

Oxygen three-isotope diagram of CM and CO bulk samples, type I and type II chondrules, CM matrix, and the anhydrous mineral separates in Murchison. The four reference lines (Y&R, PCM, CCAM, and TF lines), regression line (dashed line), and data for the CM2 and CO3 bulks, CM2 matrices, and the anhydrous mineral separates of Murchison are the same as in Fig. 1. For type I chondrule mean values, chondrules with Mg# >97 are used. For Murchison, type I chondrule average values are obtained excluding chondrule C6. For Y-81020, the average value of type I chondrules with Mg# >97 are calculated using data from Tenner et al. (2013). The 2SD uncertainties of the type I and type II chondrules are represented by ovals corresponding to the covariance matrix of $\delta^{18}O$ and $\delta^{17}O$ for each data set.

Table 1.

Mg#'s and oxygen isotope ratios of host chondrules and relict grains.

Chondrule[a]	Type-texture-relict	Mg#	+/−	n (ol, LPx, HPx)[b]	$\delta^{18}O$	unc.[c]	$\delta^{17}O$	unc.[c]	$\Delta^{17}O$	unc.[c]	$\Delta^{17}O$ 2SD
Session-1:15μm beam size											
A5	I-POP	99.5	0.2/0.1	7,0,0	−6.4	0.3	−9.3	0.3	−6.0	0.2	0.5
C2	I-PO	99.4	0.1/0.0	8,0,0	−6.2	0.4	−9.1	0.4	−5.8	0.3	0.7
A2	I-POP	99.4	0.1/0.1	4,2,0	−4.9	0.5	−8.0	0.3	−5.5	0.2	0.5
	relict ol	99.3	n.c.	1,0,0	−4.2	0.3	−7.0	0.4	−4.8	0.4	n.c.
B5	I-POP	99.3	0.2/0.0	4,2,0	−3.5	0.4	−6.9	0.3	−5.1	0.2	0.4
	relict ol	99.3	n.c.	1,0,0	−8.3	0.9†	−11.7	l.l†	−7.3	0.6†	n.c.
	relict ol	99.3	n.c.	1,0,0	−7.5	0.2	−10.6	0.3	−6.7	0.4	n.c.
C9	I-POP	99.3	0.3/0.2	6,2,0	−4.1	0.6	−7.3	0.4	−5.1	0.2	0.6
B2	I-PO	99.3	0.1/0.2	7,0,1	−4.7	0.6	−7.5	0.5	−5.0	0.3	0.6
B1	I-PP	99.2	0.1/0.1	3,4,1	−3.5	0.3	−6.7	0.2	−4.9	0.2	0.3
B7	I-PO	99.3	0.3/0.2	7,0,0	−3.3	0.5	−6.4	0.2	−4.7	0.2	0.6
A1	I-PO	99.0	0.1/0.0	3,1,0	−2.8	0.5	−5.8	0.6	−4.3	0.4	0.7
	relict ol	99.4	n.c.	1,0,0	−7.6	0.3	−9.7	0.4	−5.7	0.4	n.c.
	relict ol	99.4	n.c.	1,0,0	−7.4	0.3	−9.4	0.4	−5.6	0.4	n.c.
	relict ol	99.3	n.c.	1,0,0	−6.3	0.3	−8.7	0.4	−5.5	0.4	n.c.
A6	I-POP	99.0	0.1/0.0	0,2,0	−2.2	0.5	−5.3	0.3	−4.1	0.2	0.0
	relict ol	99.1	n.c.	1,0,0	−5.4	0.1	−8.5	0.2	−5.6	0.2	n.c.
	relict ol	99.1	n.c.	1,0,0	−5.3	0.1	−8.0	0.2	−5.3	0.2	n.c.
	relict ol	99.0	n.c.	1,0,0	−5.4	0.1	−8.6	0.2	−5.7	0.2	n.c.
	relict ol	99.0	n.c.	1,0,0	−4.8	0.1	−7.7	0.2	−5.3	0.2	n.c.
	relict ol	98.9	n.c.	1,0,0	−5.5	0.1	−8.6	0.2	−5.8	0.2	n.c.
C8	I-GOP	96.0	0.2/0.6	2,4,0	0.3	0.3	−2.6	0.3	−2.7	0.3	0.6
	relict ol	96.0	n.c.	1,0,0	−13.2	0.1	−14.7	0.3	−7.8	0.3	n.c.
	relict ol	95.9	n.c.	1,0,0	0.6	0.1	−3.1	0.3	−3.4	0.3	n.c.
Cll	II-fragment	70.3	8.0/17.2	9,0,0	2.0	0.4	−1.5	0.3	−2.6	0.2	0.2
B9	II-PO	67.0	4.7/3.8	8,0,0	1.8	0.3	−1.5	0.2	−2.5	0.2	0.4
B8	II-PO	67.5	3.1/4.9	6,0,0	2.7	0.3	−0.9	0.3	−2.3	0.2	0.1
	relict ol	96.0	n.c.	1,0,0	−5.0	0.2	−8.2	0.4	−5.6	0.4	n.c.
	relict ol	80.5	n.c.	1,0,0	−3.5	0.2	−6.9	0.4	−5.1	0.4	n.c.
Session-2 : 10 μm beam size											
B4	I-PO	99.3	0.1/0.2	7,0,0	−5.8	0.6	−9.1	0.6	−6.0	0.3	0.7
	relict ol	99.4	n.c.	1,0,0	−9.8	0.3	−13.0	0.6	−7.9	0.5	n.c.
B6	I-GO	99.1	0.2/0.2	3,2,0	−5.3	0.5	−8.7	0.4	−5.9	0.3	0.3
	relict ol	99.1	n.c.	1,0,0	−34.1	0.3	−35.6	0.6	−17.9	0.5	n.c.
	relict ol	99.0	n.c.	1,0,0	−8.8	0.3	−12.0	0.6	−7.4	0.5	n.c.
C5	I-PO	99.3	0.2/0.1	4,2,1	−5.2	0.3	−8.4	0.3	−5.7	0.2	0.4
C3	I-PO	99.3	0.2/0.2	5,2,0	−4.6	0.3	−7.7	0.3	−5.3	0.2	0.5

Chondrule[a]	Type-texture-relict	Mg#	+/−	n (ol, LPx, HPx)[b]	$\delta^{18}O$	unc.[c]	$\delta^{17}O$	unc.[c]	$\Delta^{17}O$	unc.[c]	$\Delta^{17}O$ 2SD
	relict ol	99.2	n.c.	1,0,0	−6.9	0.3	−10.0	0.4	−6.4	0.4	n.c.
Cl	I-POP	99.2	0.2/0.1	8,3,0	−3.5	0.6	−6.8	0.4	−5.0	0.2	0.6
C4	I-POP	99.2	0.1/0.1	5,3,0	−3.7	0.3	−6.8	0.3	−4.9	0.2	0.4
A3	I-POP	99.2	0.2/0.1	5,1,0	−1.8	0.4	−5.6	0.4	−4.6	0.4	0.8
C7	I-PP	99.1	0.1/0.1	1,4,3	−3.2	0.5	−6.2	0.3	−4.5	0.2	0.4
C12	II-PO	64.9	6.4/11.9	8,0,0	3.5	0.4	−0.5	0.3	−2.3	0.3	0.2
C6	I-POP	99.6	0.1/0.1	7,1,0	3.3	0.5	0.5	0.4	−1.2	0.2	0.4

[a] For each session, chondrules are sorted following decreasing host $\Delta^{17}O$ values.

[b] Numbers of mineral phases analyzed (olivine, low-Ca pyroxene, and high-Ca pyroxene).

[c] Uncertainties of host oxygen isotope ratios are propagated, combining (1) the 2SE of chondrule measurements, (2) 2SE of associated SC olivine bracketing analyses, and (3) influences from sample topography/positioning. Uncertainties of oxygen isotope ratios of relict grains are the spot-to-spot reproducibility (2SD), as determined by bracketing analyses of SC olivine.

† 2SE of the measurement (see EA4). n.c.: not calculated

Table 2.

Mg# and oxygen isotope ratios of individual grains in heterogeneous chondrules.

Chondrule Type-texture	Mg#	minerals	$\delta^{18}O$	unc.[a]	$\delta^{17}O$	unc.[a]	$\Delta^{17}O$	unc.[a]
Session-1: 15 μm beam size								
A7	99.1	ol	−5.5	0.1	−8.5	0.3	−5.7	0.3
I-POP	99.0	ol	−5.8	0.1	−9.3	0.3	−6.3	0.3
	99.1	ol	−6.7	0.1	−9.3	0.3	−5.8	0.3
	99.1	ol	−5.2	0.1	−7.9	0.3	−5.2	0.3
	99.2	ol	−10.8	0.1	−13.7	0.3	−8.0	0.3
	99.1	ol	−21.4	2.0†	−23.9	1.9†	−12.8	0.9†
	99.2	LPx	−4.9	0.1	−8.0	0.3	−5.4	0.3
	98.6	HPx	−3.2	0.1	−6.3	0.3	−4.6	0.3
Session-2: 10 μm beam size								
B3	99.1	ol	−2.4	0.3	−5.8	0.6	−4.5	0.7
I-POP	99.0	LPx	−5.2	0.3	−8.0	0.6	−5.3	0.7
	99.2	LPx	−4.5	0.3	−7.0	0.6	−4.7	0.7
	99.2	LPx	−3.2	0.3	−5.6	0.6	−4.0	0.7
	99.2	LPx	−3.4	0.3	−6.5	0.6	−4.7	0.7
	99.2	LPx	−3.2	0.3	−5.9	0.6	−4.2	0.7
	99.2	LPx	−3.0	0.3	−5.8	0.6	−4.2	0.7
	99.3	LPx	−4.7	0.3	−7.9	0.6	−5.4	0.7
	99.1	LPx	−3.7	0.3	−6.8	0.6	−4.9	0.7
A8	98.6	ol	−3.4	0.3	−6.6	0.6	−4.9	0.7
I-POP	98.9	ol	−3.3	0.3	−6.7	0.6	−5.0	0.7
	98.9	ol	−3.5	0.3	−6.7	0.6	−4.9	0.7
	98.9	ol	−2.3	0.3	−5.9	0.6	−4.7	0.7
	98.9	ol	−2.6	0.3	−5.5	0.6	−4.1	0.7
	98.9	ol	−2.1	0.3	−5.5	0.6	−4.4	0.7
	98.9	ol	−2.7	0.3	−5.5	0.6	−4.0	0.7
	99.1	LPx	−3.1	0.3	−6.1	0.6	−4.5	0.7
A4	99.5	ol	−4.7	0.3	−7.9	0.5	−5.5	0.6
I-PP	99.3	ol	−4.7	0.3	−7.6	0.5	−5.1	0.6
	99.2	ol	−7.5	0.3	−10.0	0.5	−6.1	0.6
	99.3	ol	−5.0	0.3	−8.0	0.5	−5.4	0.6
	99.4	ol	−5.3	0.3	−8.3	0.5	−5.6	0.6
	99.2	LPx	−7.4	0.3	−10.3	0.5	−6.4	0.6
	99.4	LPx	−5.3	0.3	−8.6	0.5	−5.8	0.6
	98.9	LPx	−6.2	0.3	−9.2	0.5	−6.0	0.6
	99.3	LPx	−5.5	0.3	−9.3	0.5	−6.5	0.6
CIO	99.3	ol	−3.8	0.3	−7.1	0.6	−5.1	0.6
I-GO	99.3	ol	−6.5	0.3	−9.3	0.6	−6.0	0.6
	99.3	ol	−4.2	0.3	−7.5	0.6	−5.3	0.6

Chondrule Type-texture	Mg#	minerals	$\delta^{18}O$	unc.[a]	$\delta^{17}O$	unc.[a]	$\Delta^{17}O$	unc.[a]
	99.3	ol	−5.7	0.3	−8.9	0.6	−5.9	0.6
	99.3	ol	−5.3	0.3	−7.9	0.6	−5.2	0.6
	99.4	ol	−5.5	0.3	−8.7	0.6	−5.8	0.6
	99.4	ol	−5.8	0.3	−8.8	0.6	−5.7	0.6

[a]Uncertainties of oxygen isotope ratios are the spot-to-spot reproducibility (2SD), as determined by bracketing analyses of SC olivine.

[†]2SE of the measurement (see EA4)